Journal of Medicinal Chemistry

Article

Identification and Optimization of Novel Small c-Abl Kinase Activators using Fragment and HTS Methodologies

Graham L Simpson, Sophie Marie Bertrand, Jennifer A Borthwick, Nino Campobasso, Julien Chabanet, Julia Coggins, Joshua E. Cottom, Helen C Dawson, Helen Evans, Andrew N Hobbs, Xuan Hong, Biju Mangatt, Jordi Munoz-Muriedas, Allen L Oliff, Donghui Qin, Paul T Scott-Stevens, Paris Ward, Yoshiaki Washio, Jingsong Yang, and Robert J Young

J. Med. Chem., **Just Accepted Manuscript** • DOI: 10.1021/acs.jmedchem.8b01872 • Publication Date (Web): 28 Jan 2019

Just Accepted

ACS Publications

is published by the American Chemical Society. 1155 Sixteenth Street N.W., Washington, DC 20036

Identification and Optimization of Novel Small c-Abl Kinase Activators using Fragment and HTS Methodologies

Graham L. Simpson[§⊥], Sophie M. Bertrand*[§], Jennifer A. Borthwick[§], Nino Campobasso[‡], Julien Chabanet[§], Susan Chen[†], Julia Coggins[§], Josh Cottom[‡], Siegfried B. Christensen[†], Helen C. Dawson[§], Helen L. Evans[§I], Andrew N. Hobbs[§], Xuan Hong[‡], Biju Mangatt[‡], Jordi Munoz-Muriedas[§], Allen Oliff[‡], Donghui Qin[§], Paul Scott-Stevens[§], Paris Ward[‡], Yoshiaki Washio[§], Jingsong Yang[‡], Robert J. Young[§].

[§]*GlaxoSmithKline R&D, Medicines Research Centre, Gunnels Wood Road, Stevenage, Hertfordshire, SG1 2NY, UK.*

[‡]*GlaxoSmithKline R&D, 1250 South Collegeville Road, Collegeville, PA 19426, US.*

[†]*Author deceased.*

ABSTRACT

Abelson kinase (c-Abl) is a ubiquitously expressed, non-receptor tyrosine kinase which plays a key role in cell differentiation and survival. It was hypothesised that transient activation of c-Abl kinase *via* displacement of the *N*-terminal autoinhibitory "myristoyl latch," may lead to increased hematopoietic stem cell differentiation. This would increase the numbers of circulating neutrophils and so be an effective treatment for chemotherapy-induced neutropenia. This paper describes the discovery and optimisation of a thiazole series of novel small-molecule c-Abl activators, initially

identified by high throughput screening (HTS). Subsequently, a scaffold-hop, which exploited the improved physicochemical properties of a dihydropyrazole analogue identified through fragment screening, delivered potent, soluble, cell-active c-Abl activators, which demonstrated intracellular activation of c-Abl *in vivo*.

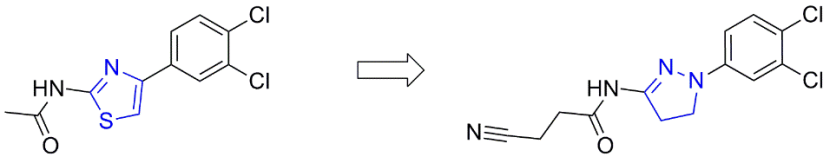

2
FP Binding pIC_{50}: **6.5**
Cell Act pEC_{50}: **4.5**

HTS Hit

32
FP Binding pIC_{50}: **6.5**
Cell Act pEC_{50}: **6.1**

Showed *in vivo* target engagement and pathway activation

INTRODUCTION

Kinases are key nodes in signal transduction pathways, modulating the phosphorylation of pertinent hydroxyl residues on target proteins.[1] Their activity is tightly regulated *in vivo* by a combination of mechanisms, including phosphorylation, sub-cellular trafficking and conformational control.[2,3] Whilst considerable research efforts have led to the discovery of small molecule kinase *inhibitors* (over 28 approved),[4] lesser progress has been made with discovery of small molecule *activators* of protein kinases. This mechanism has been shown to be able to modulate activity in several biologically relevant targets, leading to increased downstream signalling and potentially therapeutically useful pharmacological modulation.[5]

Abelson kinase (c-Abl) is a ubiquitously expressed, non-receptor tyrosine kinase which plays a key role in cell differentiation and survival.[6] It is well known that patients with

the Philadelphia chromosome (Ph1) express an aberrant, constitutively active, fusion protein of Abl, BCR-Abl, which results in uncontrolled neutrophil proliferation, the clinical symptoms of chronic myelogenous leukaemia (CML).[7, 8] These patients can be treated effectively by the ATP-competitive kinase inhibitors Imatinib, Nilotinib or Dasatinib (Figure 1).[9,10]

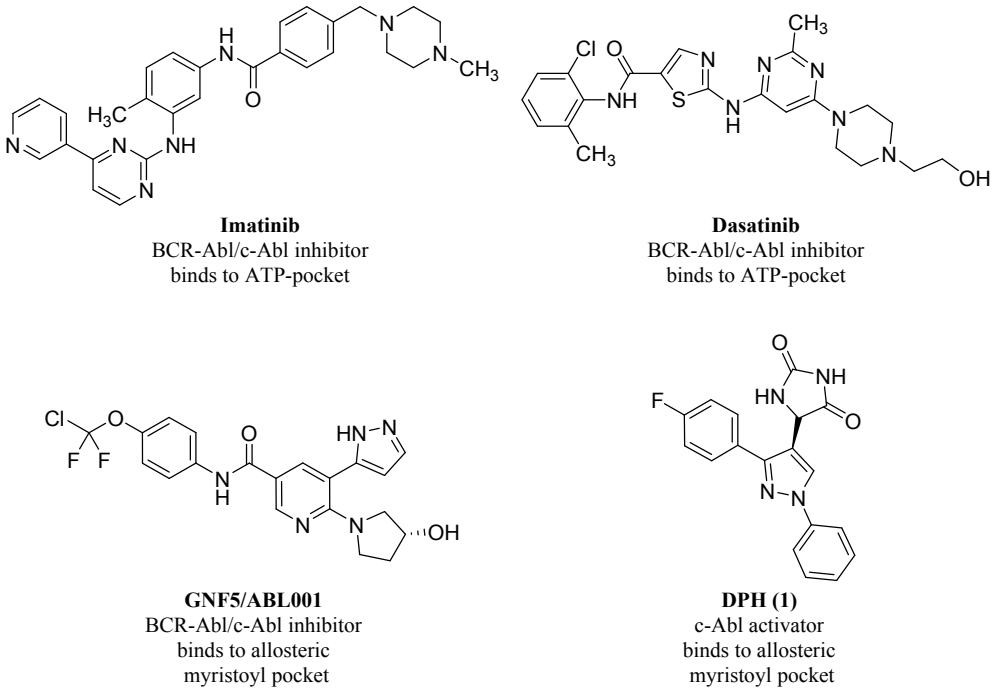

Figure 1. Published c-Abl kinase inhibitors and activators – (a) ATP-competitive inhibitors Imatinib and Dasatinib; (b) allosteric inhibitor GNF5/ABL001; (c) allosteric activator DPH (**1**).

c-Abl (1b isoform) is mostly present in an autoinhibited, compact, inactive, conformation maintained by binding of the N-terminal 1-82 residues "myristoyl latch" to a lipid pocket in the kinase domain (Figure 2).[11,12] Allosteric inhibitors of c-Abl kinase,[13] also active against BCR-Abl, GNF-2,[14] GNF-5/ABL001,[15,16] have been described which bind at this myristoyl pocket, stabilising interaction with the kinase domain helix αI' and mimicking the autoinhibited conformation of c-Abl. (Figure 1). Concurrently, our group have previously described the discovery of a small molecule

activator of c-Abl kinase, DPH (**1**), which binds at the same pocket, displacing the myristoyl latch and leading to cellular activation (Figure 1).[17] Activators of c-Abl kinase have potential therapeutic applications in chemotherapy-induced neutropenia,[18,19] breast[20] and prostate[21] cancer and ischemic injury.[22] Interestingly, combination of c-Abl activator, DPH (**1**), and ATP-competitive BCR-Abl inhibitor Imatinib, has been shown to be synergistic, hypersensitising BCR-Abl1 leukaemia cells in CML.[23]

Activators of c-Abl were identified within GSK by high throughput screening and the biology around small molecule activator DPH (**1**) was previously reported.[17] This paper describes the discovery of a series of pyrazoline activators of c-Abl kinase and their medicinal chemistry optimisation as tool molecules for further *in vivo* investigations.

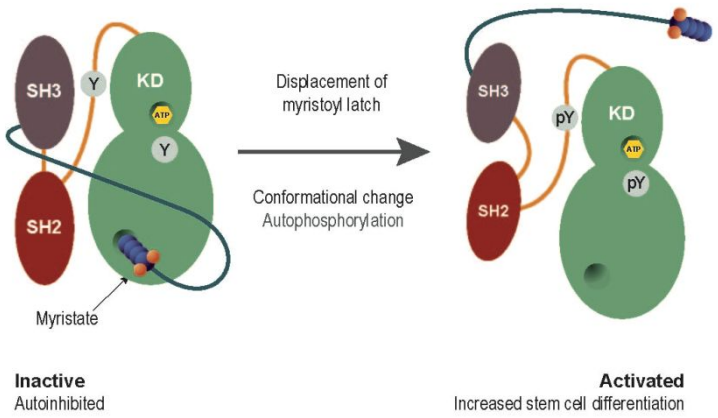

Figure 2. Activation of c-Abl kinase by relieving inactive, autoinhibited conformation. In the autoinhibited form the tyrosine residues (Tyr245 and Tyr412) are inaccessible to phosphorylation. Upon displacement of the N-terminal myristoyl latch from the hydrophobic pocket in the kinase domain, a conformational change occurs allowing autophosphorylation of these residues and increased kinase activation. (Abbreviations: KD=kinase domain; SH2/SH3=Src-homology domain 2/3; Y=tyrosine; pY=phosphotyrosine; ATP=adenosine triphosphate).

RESULTS AND DISCUSSION

Aminothiazoles **2** and **3** (Figure 3) were identified by high throughput screening, which utilised an assay based on immobilized metal affinity for phosphochemicals (IMAP),[24] configured to find molecules which increase the activation of c-Abl tyrosine kinase. This was used to screen a diverse set of 1.3 million compounds.[24] Additionally, a complementary fluorescence polarisation (FP) assay monitored competitive displacement of a fluorescent-tagged myristoylated peptide from the kinase-dead mutant enzyme, N-terminal truncated c-Abl$^{46-534}$(D382N)[17] which was used for follow-up screening. This peptide is known to bind into the kinase domain and its displacement confirmed the allosteric mechanism of kinase activation. Cellular activity was assessed by Western Blot detection of the phosphorylation of full-length c-Abl (pY245, pY412) from HEK-MSRII cell lysates.[24] In common with the previously disclosed c-Abl activator, DPH (**1**), compounds in this paper were shown to be myristoyl-competitive activators of full-length, autoinhibited c-Abl enzyme (c-Abl-1b$^{1-531}$) *in vitro* (FP and IMAP assays).[24] The initial hits also displayed some cellular activation, although at a low level which required optimisation. The key objectives of the medicinal chemistry programme focussed on exploring the structure-activity relationships around the template and improving the intracellular activation.

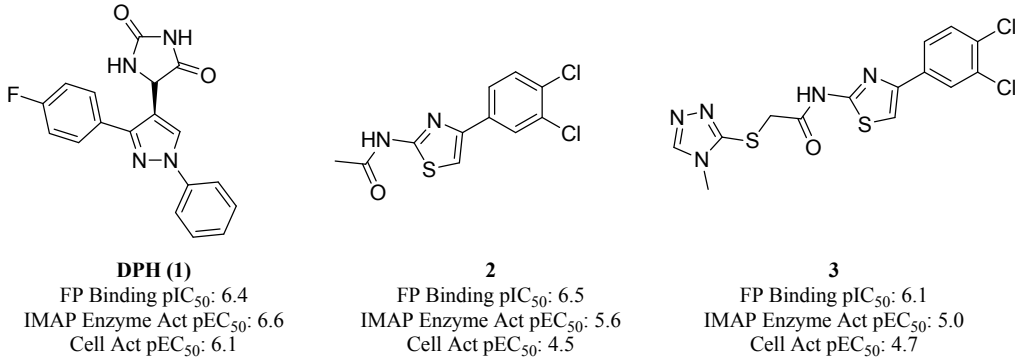

Figure 3. Structure and c-Abl activation data for aminothiazoles **2** and **3** with comparison to previously published pyrazole activator DPH (**1**).[9]

Initially, the SAR of amide substituents on the left-hand side of the molecule was delineated; by maintaining the dichlorophenyl group identified in the hits **2** and **3**. These changes resulted in increased enzyme binding affinity and activation (Table 1 **- 4-10**). As is often seen with small molecule-ligand interactions, increasing lipophilicity led to an increase in potency (*e.g.* **4**). Modification of the amide to a sulphonamide (**10**) led to a reduction in activation. However, introduction of hydrogen-bond acceptors, was favoured (*e.g.* **6-9**). In general, the compounds showed poor cellular activation, with **5** and **6** showing the highest cellular activity of any of the compounds tested. Most of the compounds displayed reasonable permeability in an artificial membrane assay (AMP) but they also generally had poor physical properties, indicated by their low solubilities, which likely contributed to their relatively poor cellular activity.

Table 1. Amide Modification on the Thiazole Series

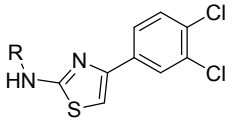

Cmpd	R	IMAP[a] Enzyme activation (pIC_{50})	FP[b] Myristoyl binding (pIC_{50})	Cellular[c] activation (pEC_{50})	CLND[d] (μM)	AMP[e] (nm/sec)
1[f]	-	6.6	6.4	6.1	>395	350
2		5.6	6.5	4.5	<1	196
4		6.8	6.6	<4.3	3	227
5	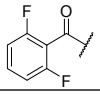	6.6	6.5	5.3	5	<30
6	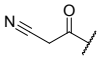	5.9	6.3	5.3	57	142
7		6.3	6.7	<4.3	2	61
8	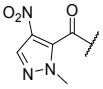	7.5	6.7	4.8	<1	260
9		6.4	6.7	<4.3	20	370
10		4.6	<4.3	<4.3	429	220

n numbers ≥2. [a]Assays performed using an end-point activation IMAP protocol; [b]Fluorescence Polarization (FP) competition binding assay; [c]In-cell Western (ICW) assay using Bacmam transduced HEK-MSRII cells.[17] [d]CLND solubility refers to kinetic solubility measured using chemiluminescent nitrogen detection - >100 ± 30 μM is defined as good solubility. [e]AMP refers to artificial membrane permeability measured using black-lipid membrane - >200 ± 30 nm/sec is defined as good permeability (See Supporting Information). [f]data have been reported previously.[17]

To complement the knowledge gained from the chemical variation in the series, crystal structures of allosteric inhibitor GNF-2[14] and activator **6**, soaked into crystals of human c-Abl kinase domain, were obtained. There were two molecules in the asymmetric unit and both myristoyl pockets were fully occupied. As shown previously in the mouse

form of c-Abl,[14,16] the αI'-helix was bent down towards the GNF-2 molecule (Figure 4). In these structures, only one of the molecules in the asymmetric unit showed the αI'-helix to be bent with GNF-2 whereas the other molecule had the αI'-helix involved in a crystal contact and could not bend to interact with GNF-2. The crystal structure of activator **6** showed that the molecule bound to the myristoyl pocket and pushed the αI'-helix into an extended conformation away from the myristoyl pocket. There was also a key 2.8Å hydrogen-bond formed with the backbone Ala452, at the C-terminus of αF-helix, to Ala462 and to the guanidine of Arg351. The hydrogen-bond with Arg351 was absent with DPH (**1**) highlighting the more efficient polar interactions in this compound.[17] The dichlorophenyl group showed good shape complementarity in a lipophilic pocket defined by residues Leu359, Leu360, Ala363, Val487, Leu448, and Phe512. To accommodate the larger dichlorophenyl ring, Leu360 and Phe512 adopted alternative conformations compared to the bound structure of DPH (**1**). The aminothiazole ring occupied the entrance area at the back of the myristoyl pocket, sandwiched between the N-term of αE-helix and loop Pro380-Pro384 with no observable hydrogen-bond interactions. The cyanomethyl picked up a strong hydrogen-bond with the guanidine of Arg351, a common feature of inhibitors in this series. The αI-helix, thought to be essential to maintain c-Abl in its inactive form was clearly displaced. Superposition of aminothiazole **6** and pyrazole DPH (**1**) X-ray crystal structures showed that the displaced Leu360 in the aminothiazole pushes the αI-helix further out than in the pyrazole DPH (**1**) and disrupted the SH3-SH2 packing against the kinase domain.

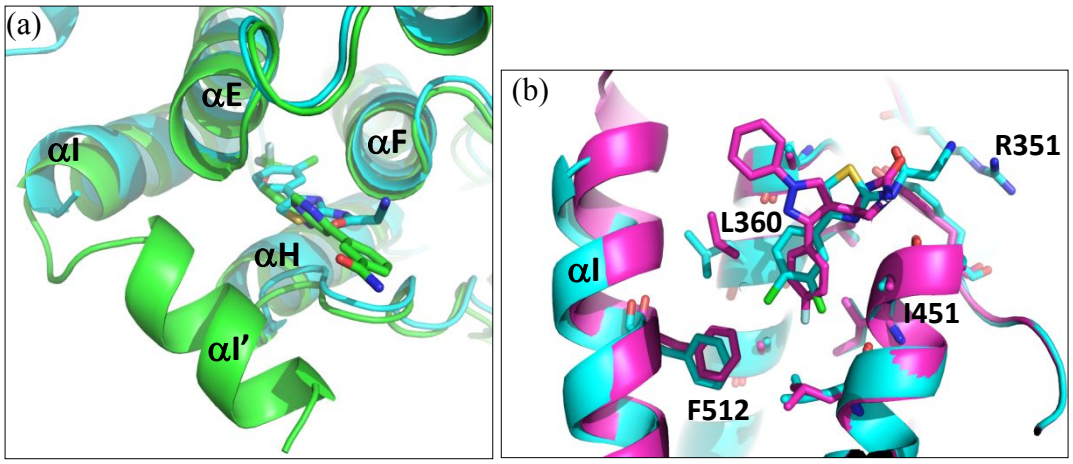

Figure 4. (a) Overlay of c-Abl kinase domain crystal structures of GNF-2[14] (green – PDB code 3K5V) and **6** (cyan – PDB code 6NPE) showing the difference between the positions of the αI'-helix. (b) Overlay of X-ray crystal structure of **6** c-Abl (kinase domain) with DPH (**1**) (pink - PDB code 3PYY). Leu360 and Phe512 are rendered as sticks and highlight the difference between respective lipophilic pockets and the shift in αI-helix.

Next, the SAR around the right-hand side of the molecule, the 3,4-dichlorophenyl functionality of **2**, was investigated, through synthesis of thiazole analogues wherein the left-hand side *N*-acetamide motif was maintained. The biochemical assay data and physical measurement of these compounds are summarised in Table 2, wherein the 3,4-dichlorophenyl group in **2** was found to be optimal for activity, as simple changes (H **11** and **12**, F **13** and **14**, Me **15**) resulted in significant loss of activation. Other modifications designed to improve solubility through the introduction of polar groups, such as a hydroxyl in **16,** were also not tolerated. Similarly, replacement of the phenyl ring with heterocycles (**17-19**) gave a reduction in potency even though solubility was increased in some cases (*e.g.* **19**). Interestingly, compound **15** demonstrated a marked difference between its binding and enzyme activation, suggesting that the modification may possibly have led to a crossover between the activation and inhibition.

Table 2. Dichlorophenyl Moiety SAR

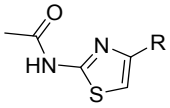

Cmpd	R	IMAP[a] Enzyme activation (pIC_{50})	FP[b] Myristoyl binding (pIC_{50})	Cellular[c] activation (pEC_{50})	CLND[d] (µM)	AMP[e] (nm/sec)
2	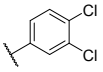	5.6	6.5	4.5	<1	196
11	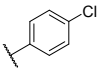	4.5	5.0	ND	1	250
12	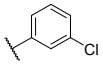	5.1	<4.3	ND	2	340
13	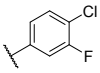	5.5	6.1	4.3*	5	350
14	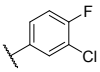	4.4	5.6	<4.3*	10	94
15	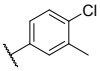	4.5	6.1	<4.3	1	140
16	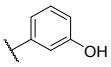	<4.3	4.9	ND	103	270
17	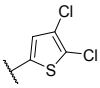	<4.0	5.2	<4.3	1	280
18	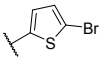	4.9	5.3	<4.3	16	210
19		<4.0	<4.3	ND	186	250

n numbers ≥2 unless stated *n=1. [a]Assays performed using an end-point activation IMAP protocol; [b]Fluorescence Polarization (FP) competition binding assay; [c]In-cell Western (ICW) assay using Bacmam transduced HEK-MSRII cells.[17] [d]CLND solubility refers to kinetic solubility measured using chemiluminescent nitrogen detection - >100 ± 30 µM is defined as good solubility. [e]AMP refers to artificial membrane permeability measured using black-lipid membrane - >200 ± 30 nm/sec is defined as good permeability.

From this SAR exploration, it was concluded that the dichlorophenyl group was likely to be close to optimal, so it was decided to focus future efforts on the core of the molecule. Thus, a range of 5-membered and 6-membered rings (**20**-**27**), which were predicted to place the substituents along similar vectors to the aminothiazole template, was investigated (Table 3).

Table 3. Thiazole Core Modification

Cmpd	Structure	IMAP[a] Enzyme activation (pIC_{50})	FP[b] Myristoyl binding (pIC_{50})	Cellular[c] activation (pEC_{50})	CLND (µM)	AMP (nm/sec)
6	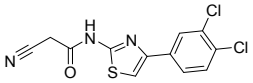	**5.9**	**6.3**	**5.3**	**57**	**142**
20	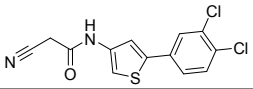	**4.8**	**5.4**	**<4.3**	**10**	**120**
21	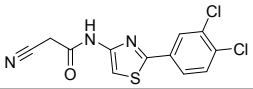	**5.8**	**6.9**	**4.8**	**2**	**350**
22	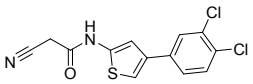	**5.5**	**5.4***	**4.7**	**12**	**190**
23	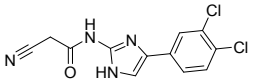	**5.8**	**6.2**	**5.5**	**14**	**310**
24	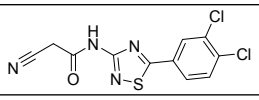	**5.7**	**5.6**	**4.8**	**69**	**280**
25	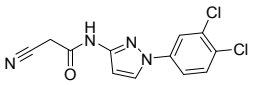	**5.6**	**5.8**	**5.1**	**34**	**310**
26	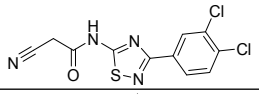	**5.5**	**6.0**	**5.0**	**370**	**230**
27	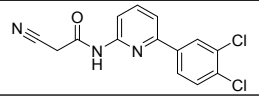	**4.9**	**5.8**	**<4.3**	**1**	**215**

n numbers ≥2 unless stated *n=1. [a]Assays performed using an end-point activation IMAP protocol; [b]Fluorescence Polarization (FP) competition binding assay; [c]In-cell Western (ICW) assay using Bacmam transduced HEK-MSRII cells.[17] [d]CLND solubility refers to kinetic solubility measured using chemiluminescent nitrogen detection - >100 ± 30 µM is defined as good solubility. [e]AMP refers to artificial membrane permeability measured using black-lipid membrane - >200 ± 30 nm/sec is defined as good permeability.

Disappointingly, the cellular activity and, with the exception of 1,2,4-thiadiazole **26**, solubility of the analogues were not improved across the board. At this point, it was apparent that the chemistry strategy was largely pursuing compounds with rather poor physical properties, especially low solubility (generally < 20 μM) associated with relatively high lipophilicity and proportion of sp^2-hybridised heavy atoms. In Table 2 it was apparent that the dichlorophenyl motif was likely to be optimal and in Table 3 (compounds **20**-**27**) the isosteric replacements for the 2-aminothiazole all maintained the planarity of the molecule and resulted in generally poor translation of intrinsic potency into cellular potency. These observations were consistent with the growing body of evidence indicating the consequences of working with overtly lipophilic and/or high sp^2/high aromatic ring count molecules, which are poorly soluble, may have poor permeation and other developability risks. Lipophilicity is the antithesis of aqueous solubility and is associated with non-specific entropically-driven binding.[25,26] It has been shown that in many developability assays aromatic ring count *per se* or the proportion of sp^2 atoms is indicative of similar risks and that, the former count has an additive risk with lipophilicity values in many assays.[27]

Almost concurrently, synthetic concepts to address the planarity issues were complemented by the output of a fragment screening initiative, which identified pyrazoline **28** as a low micromolar activator of c-Abl (Table 4). Gratifyingly, acetylation and cyanoacetylation to give compounds **29** and **30** showed increased binding and effective activators were quickly identified. The generation of a X-ray structure with **29** (PDB code 6NPU) showed a similar binding mode to the aminothiazole series (Figure 5), but importantly displayed a conformational twist in the core due to the smaller ring and the reduced sp^2 character. Such modifications led to a significant improvement in melting point (Table S1), solubility and cell potency, with

much improved kinetic solubility.[28] Reduction in aromaticity of drug molecules has been shown to improve physicochemical properties such as solubility and has been associated with a lower incidence of attrition during drug development.[27,29,30] In the pyrazoline series the improved physical properties were manifested through enhanced solubility and permeability compared with the more sp^2-rich analogues, which led to a lower drop-off in potency between the biochemical and cell activation assay. The aminopyrazoline core was relatively stable to oxidation to the pyrazole with no decomposition observed during storage in solution or as solid **28**.[31,32] Matched pair data also showed that the pyrazole analogues had lower activities (e.g. **25** *vs* **30**).

Table 4. Pyrazoline Series

Cmpd	Structure	IMAP[a] Enzyme activation (pIC_{50})	FP[b] Myristoyl binding (pIC_{50})	Cellular[c] activation (pEC_{50})	CLND[d] (µM)	AMP[e] (nm/sec)
28	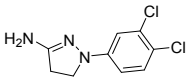	**5.2**	**5.7**	**4.9**	**69**	**320**
29	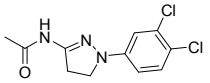	**6.5**	**6.4**	**6.1**	**31**	**360**
30	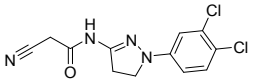	**6.6**	**6.4**	**6.0**	**202**	**320**

n numbers ≥2. [a]Assays performed using an end-point activation IMAP protocol; [b]Fluorescence Polarization (FP) competition binding assay; [c]In-cell Western (ICW) assay using Bacmam transduced HEK-MSRII cells.[17] [d]CLND solubility refers to kinetic solubility measured using chemiluminescent nitrogen detection - >100 ± 30 µM is defined as good solubility. [e]AMP refers to artificial membrane permeability measured using black-lipid membrane - >200 ± 30 nm/sec is defined as good permeability.

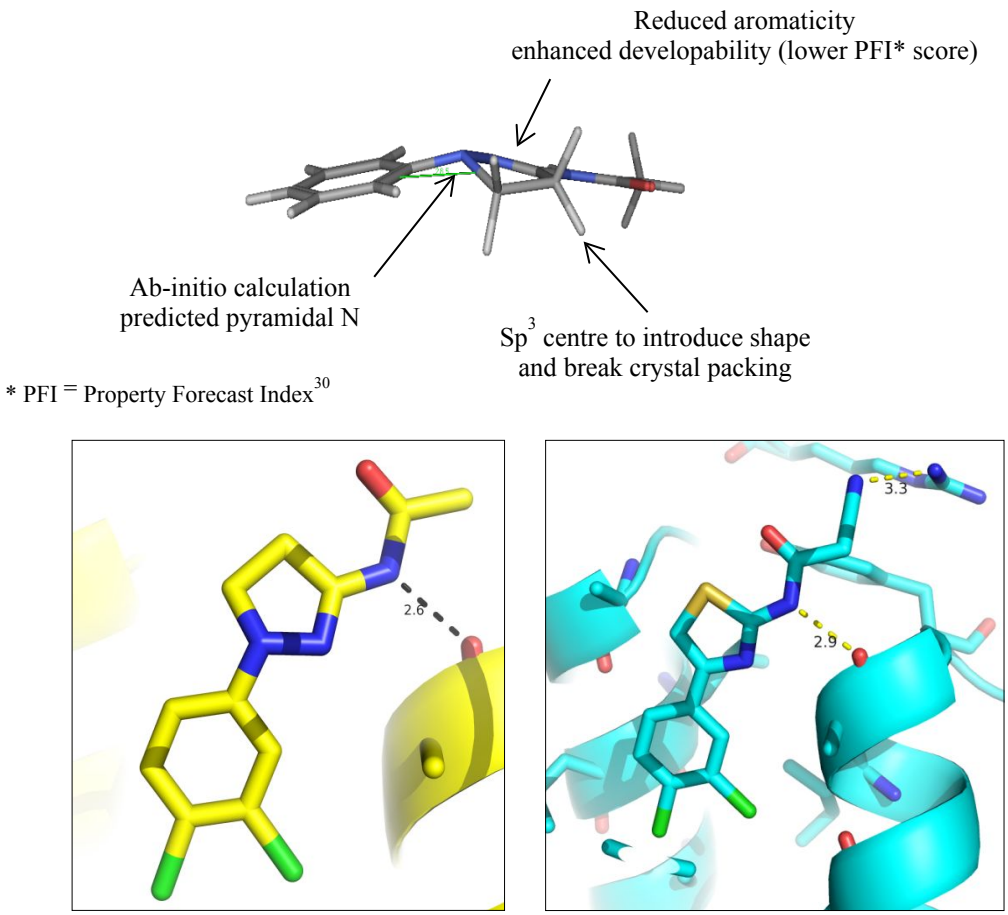

Figure 5. Aminopyrazoline series (**29**, left – PDB code 6NPU) has lower lipophilicity and increased cellular activation compared to aminothiazoles (**6**, right – PDB code 6NPE). H-bond to backbone Ala452 is indicated by dashed lined and annotated with distance (Å).

Optimisation of the pyrazoline series. The similarity in binding mode with the aminothiazole series allowed a rapid transfer of SAR. A range of substituted aromatic and alkyl amides were well tolerated with the pyrazoline core (Table 5). Acetamide **29** demonstrated good affinity and efficacy in the enzyme assays although it displayed poor aqueous solubility. To further improve the molecule's overall physicochemical profile, polar functional groups were introduced on the amide. The introduction of a hydrogen-bond acceptor to interact with Arg351 was expected to improve potency and solubility. Cyanoacetamide **30** achieved excellent solubility with a similar level of potency to the acetamide. An acyclic acetamide analogue **31** (only *S*-enantiomer tested)

only demonstrated moderate potency, in contrast to a cyclic lactam analogue **33** (tested as racemate), which achieved an excellent potency in the enzyme efficacy assay. It was postulated that the limited rotation of the cyclic amide constrained the vector for hydrogen bonding towards Arg351. Solubility may have been improved due to decreased propensity to form infinite ladders of intermolecular hydrogen-bond interactions between *cis*-amides in the solid state.[16]

Aromatic amide derivatives were explored in more detail. The 3- and 4-pyridyl amide analogues, **34** and **35**, showed significantly improved activation in the enzyme assay compared to isoelectronic 2-pyridyl amide, **36**. Further exploration of this result suggested that introduction of nitrogen atoms at the 2-position of the ring reduced potency even if the 3- or 4-position nitrogen was retained (**37**, **38**). These results were reinforced with the pyridazine **39** and pyrimidine **40**. A CH in the 2- and 6-position of the ring was expected to cause a slightly twisted conformation to avoid steric clash between the amide NH and aromatic CH, enhancing the hydrogen-bond with Arg351 as was seen with the difluorophenyl amide **5** in the aminothiazole series. In addition, an intramolecular hydrogen-bond between the 2-pyridyl nitrogen and the amide was predicted to disrupt the hydrogen-bond of the amide NH to the enzyme pocket, thereby introducing a planar conformation with a reduction in cell activity. The retention of enzyme potency with 2,6-difluorophenyl derivative **41** would suggest a significant contribution of a conformational preference, although a slightly lower cell potency was observed. Based on these results, the 2-fluoro-3-pyridyl (**42**), 3-fluoro-4-pyridyl (**43**) and 4-methyl-5-pyrimidyl (**44**) analogues were synthesised and **44** was found to have the highest potency to date (pEC_{50} = 7.4).

Table 5. Amide Modification on the Pyrazoline Series

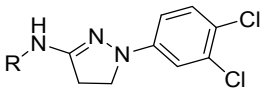

Cmpd	R	IMAP[a] Enzyme activation (pIC_{50})	FP[b] Myristoyl binding (pIC_{50})	Cellular[c] activation (pEC_{50})	CLND[d] (µM)	AMP[e] (nm/sec)
29		6.5	6.4	6.1	31	360
30	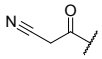	6.6	6.4	6.0	202	320
31	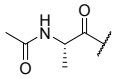	5.8	5.9	5.1	58	340
32	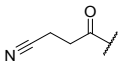	6.6	6.5	6.1	39	355
33	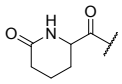	6.4	6.3	5.6	416	250
34	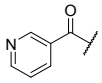	6.8	6.6	6.2	4	305
35	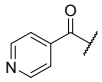	6.7	6.5	5.8	9	303
36	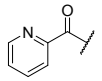	5.7	5.7	<4.3	11	350
37	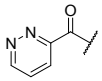	5.3	6.1	<4.3*	67	ND
38	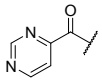	4.8	6.0	4.4*	13	320
39	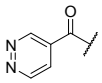	6.6	6.3	6.3	23	360
40	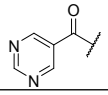	6.6	6.3	6.2	8	350
41	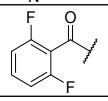	6.2	6.4	5.5	ND	ND
42	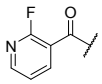	6.9	6.4	5.9	13	570
43	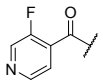	6.9	6.7	5.8	36	280
44	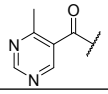	7.4	6.8	6.5	12	340

n numbers ≥2 unless stated *n=1. [a]Assays performed using an end-point activation IMAP protocol; [b]Fluorescence Polarization (FP) competition binding assay; [c]In-cell Western (ICW) assay using Bacmam transduced HEK-MSRII cells.[17] [d]CLND solubility refers to kinetic solubility measured using chemiluminescent nitrogen detection - >100 ± 30 μM is defined as good solubility. [e]AMP refers to artificial membrane permeability measured using black-lipid membrane - >200 ± 30 nm/sec is defined as good permeability.

Based on computational modelling (multi-component solvent search, MCSS) it was proposed to exploit a small hydrophobic pocket from the substituent positions on the pyrazoline ring.[33] To probe this binding site, substitution of the pyrazoline ring with a methyl group was investigated. Four possible methyl substituted isomers at the 4- or 5-position of the pyrazoline ring were prepared (racemate **45**, (*R*)-5-Me **48**, (*S*)-5-Me **49**, (*R*)-4-Me **46**, (*S*)-4-Me **47**). As predicted by molecular modelling, only the (*S*)-4-Me analogue **47** demonstrated a small improvement in potency (pIC_{50} = 6.9). To attempt to introduce further hydrogen-bond interactions, the backbone NH of Ala356 was targeted by building from the 4-(*S*)-methyl group. Calculation of the distance between NH and CH_3 suggested a hydroxyethyl group at the 4-position could make a positive hydrogen bonding interaction whilst minimising the increase of lipophilicity. Hydroxyethyl analogues, **50** and **51** both demonstrated a similar level of potency in the enzyme assay as the racemate with significantly improved solubility but unfortunately led to lower cellular activation (Table 6). The X-ray crystallography of **51** confirmed that the terminal OH successfully made a hydrogen-bond interaction with backbone NH *via* a water molecule (Figure 6). Although *in vitro* enzyme activation had been maintained it did not translate to the cellular assay. Combination of the optimal (*S*)-methylated core with a preferred pyrimidine amide group afforded **52** with an enzyme potency of pEC_{50} = 7.7 and a cellular efficacy of pEC_{50} = 7.0, representing the most active compound synthesised.

Table 6. Exploration of Pyrazoline Core Substitution

Cmpd	Structure	IMAP[a] Enzyme activation (pIC_{50})	FP[b] Myristoyl binding (pIC_{50})	Cellular[c] activation (pEC_{50})	CLND[d] (µM)	AMP[e] (nm/sec)
29	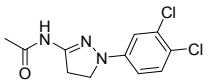	6.5	6.4	6.1	31	360
34	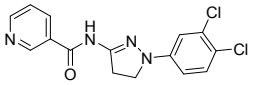	6.8	6.6	6.2	4	305
35	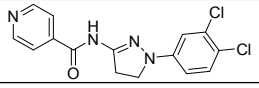	6.7	6.5	5.8	9	303
45	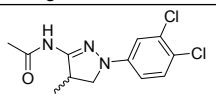	6.6	6.1	6.3	49	405
46	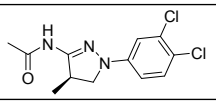	5.6	5.4	4.7	36	380
47	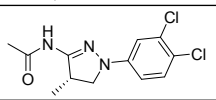	6.9	6.4	6.2	32	420
48	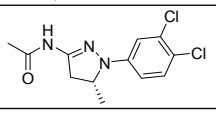	5.7	5.8	5.0	173	410
49	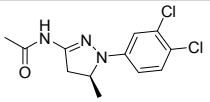	6.3	6.4	5.0	125	420
50	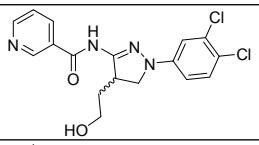	6.9	6.6	5.1	192	190
51	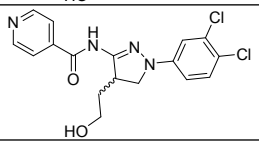	7.0	6.8	5.5*	167	335
52	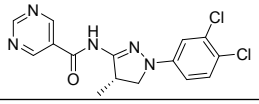	7.7	6.5	7.0	9	420

n numbers ≥2 unless stated *n=1. [a]Assays performed using an end-point activation IMAP protocol; [b]Fluorescence Polarization (FP) competition binding assay; [c]In-cell Western (ICW) assay using Bacmam transduced HEK-MSRII cells.[17] [d]CLND solubility refers to kinetic solubility measured using chemiluminescent nitrogen detection - >100 ± 30 µM is defined as good solubility. [e]AMP refers to artificial membrane permeability measured using black-lipid membrane - >200 ± 30 nm/sec is defined as good permeability.

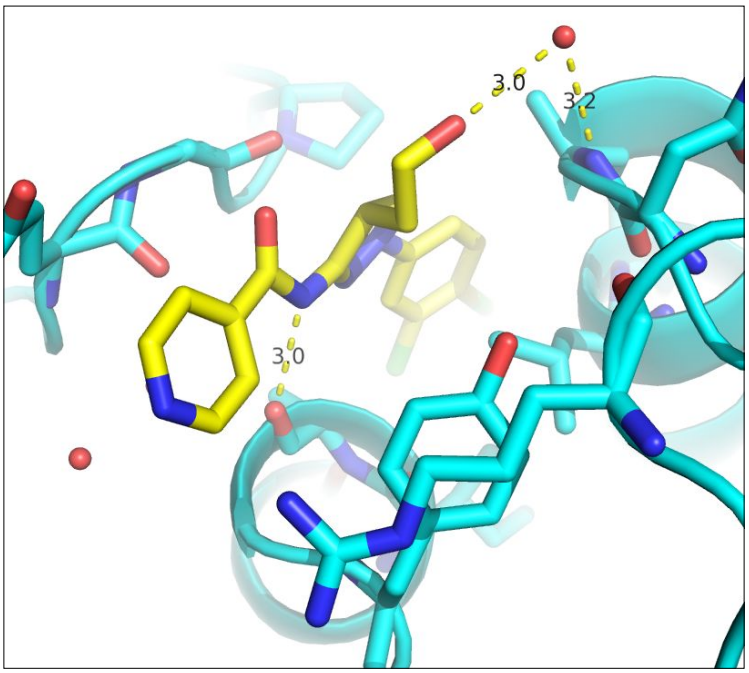

Figure 6. Crystal structure of c-Abl kinase domain with **51** showing a bridging water molecule between hydroxyl group and amide backbone – PDB code 6PNV.

***In Vivo* c-Abl Activation.** In order to evaluate if small molecule c-Abl activators were able to activate endogenous c-Abl *in vivo*, comparative studies of three equipotent compounds in the cellular activation assay (**1**, **32** and **45**) from different series were undertaken in mice.[17] The microsomal intrinsic clearance (mL/min/mg protein) was determined in pooled CD1 mouse liver microsomes and compared to measurement of compound concentrations in terminal mouse plasma samples at two different timepoints (40 min and 180 min), following Intraperitoneal injection (100 mg/kg, 10 mL/kg, n=4 mice per compound) of formulated compounds. Concurrently phosphorylation of c-Abl substrate, Crk-L, in the blood samples was measured as an indication of the level of c-Abl activation *in vivo*. Crk-L is a well-characterized cellular substrate of active c-Abl.

Table 7. c-Abl Activator mouse plasma concentrations and increase in c-Abl phosphorylation of substrate Crk-L after

				In Vivo Plasma Concentration (ng/mL)[a]		Fold Increase phCRKL Vs Total Crk-L (normalised)[b]	
Cmpd	**Structure**	**cellular activation (ICW EC_{50})**	***In Vitro* Clearance[c] (mL/ min/ mg protein)**	**40 min**	**180 min**	**40 min**	**180 min**
1	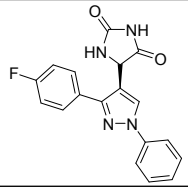	6.1	0.266	15100 ± 1150	1050 ± 595	13x	28x
45	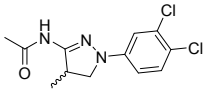	6.3	0.408	5540 ± 233	2540 ± 143	1x	5x
32	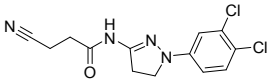	6.1	< 0.01	15600 ± 1700	17600 ± 3530	19x	35x

[a] *Terminal Plasma concentrations (Mean ± SEM) based on n=4 mice/time point;* [b]*The phCrk antibody utilized recognizes pY221 of Crk and pY207 of Crk-L, a Crk isoform and values are quoted as a ratio of pCrk-L to total Crk, normalised to background ratio (phCrk-L/Crk = 0.001);* [c]*Intrinsic clearance determined in CD1 mouse liver microsomes (final protein concentration 0.5 mg/mL, drug concentration 0.5μM, 1 h incubation).*

Control compound DPH (**1**) was metabolised rapidly *in vitro*. Compound **45** had a significantly higher turnover in the *in vitro* microsomal assay (0.408 mL/min/mg protein) showing a clear metabolic liability from the introduction of the methyl group into the pyrazoline core. In contrast, compound **32** showed good metabolic stability over 1 hour *in vitro*. This trend was borne out *in vivo* with compound **45** showing only moderate plasma levels at the 40-minute time-point, whereas compounds **32** and **1** showed ~ 3-fold higher plasma exposure. At the 180-minute time-point, both compounds **1** and **45** were reduced to low levels (<5000 ng/mL) with compound **32** showing sustained high levels (17600 ng/mL).

Gratifyingly the plasma drug levels correlated well with the observed activation of c-Abl confirming target engagement *in vivo*. Compounds **1** and **32** both demonstrated increased activation of c-Abl kinase resulting in higher levels of the product phCrk-L at both the 40-minute and 180-minute time-points (13-fold to 35-fold over vehicle). Interestingly, phCrk-L levels were still increased at the 180-minute time point even with low drug levels of compound **1** (1050 ng/mL), showing the potential for catalytic autoactivation of c-Abl *in vivo*.[34] Further investigation of compound **32** in a chronic dosing *in vivo* model (oral, 100 mg/kg BID for 10 days) was attempted to understand the effect of increasing c-Abl activity on neutrophil levels as a potential treatment for chemotherapy-induced neutropenia. Unfortunately, the study was halted due to significant levels of haemolysis being observed before the efficacy could be assessed. Although 3-aminopyrazoline templates have been exemplified as anti-inflammatory compounds in the literature,[35-37] there are reports of a similar compound showing induction of methemoglobinemia, and haemolytic anaemia in rats at higher doses,[38] which may suggest compound rather than mechanism-related toxicity. Further studies would be required to fully elucidate the mechanism of toxicity.

In this work, biochemical, biophysical and cellular assays were configured to identify a novel, myristoyl competitive series of *activators* of c-Abl which led to increased phosphorylation in cellular systems and *in vivo*.[17,24] X-ray crystallography indicates that these molecules bind in the myristoyl pocket of c-Abl-1b, displacing the myristoyl tail, forcing the αI-helix of the C-terminus. This contrasts with discovered allosteric inhibitors of BCR-Abl, GNF-2 and GNF-5,[14,39] which bind in the same myristoyl pocket but stabilise the inactive conformation of BCR-Abl by forming key H-bonding

interactions with the αI-helix of the C-terminus. This mechanism, first demonstrated in c-Abl has so far not been shown to operate in other kinases.

CONCLUSIONS

In summary, a novel aminopyrazoline series of direct small molecule activators of autoinhibited c-Abl kinase has been discovered, which may be developed as treatments for chemotherapy induced neutropenia. SAR was optimised using crystallography to guide synthesis leading to potent cell-active compounds with a balance of physicochemical properties. By focussing on physicochemical properties, improved solubility and cell potency the aminodihydropyrazole template was discovered which showed favourable binding kinetics at the target and higher cellular potency. The compounds showed *in vivo* target engagement and pathway activation although could not be developed further into oral medicines due to *in vivo* toxicity. These molecules may be useful as tools and to develop further as therapeutics for chemotherapy induced neutropenia.

CHEMISTRY

The compounds reported in this paper were prepared by a variety of methods from commercially available starting materials.

Compounds **2** and **4-10** were synthesised following Scheme 1. The 4-(3,4-dichlorophenyl)thiazol-2-amine intermediate **54** was prepared *via* the Hantzsch thiazole condensation of the bromoketone **53** with thiourea.[40] The amide formation was carried out using the *in situ* generated acid chloride[41] or HATU-mediated conditions to afford analogues **2** and **4-9** (Scheme 1). The sulphonamide analogue **10** was prepared using reaction of methylsulfonyl chloride. Isolated yields were low but acceptable for initial investigation of SAR.

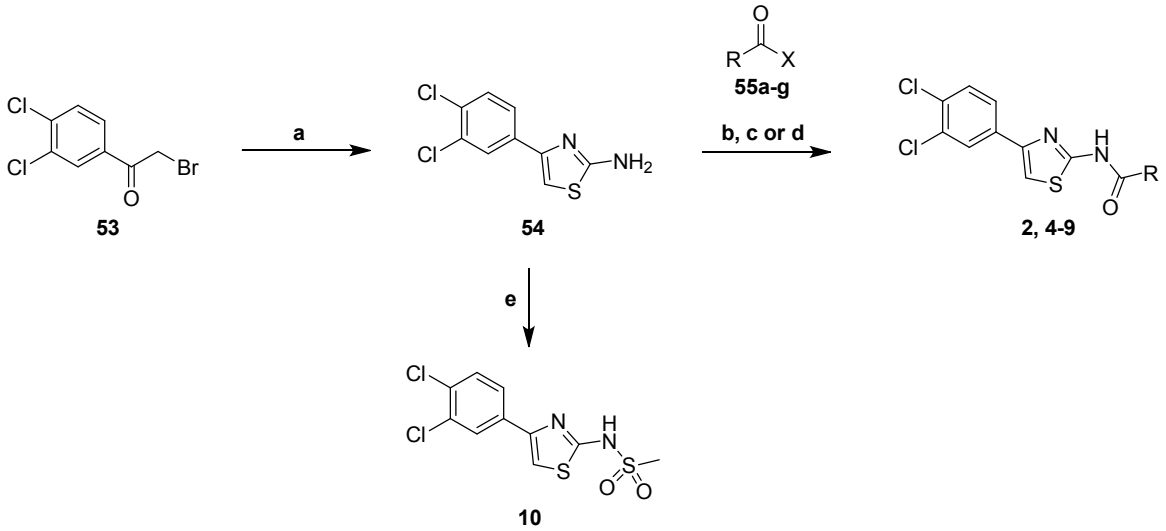

Scheme 1. Amide and Sulphonamide Formations using Aminothiazole Core

Reagents and conditions: (a) thiourea, EtOH, rt, 10 min, 85%; (b) HATU, DIPEA, DMF, 50 °C, 2-65 h, 9-33%; (c) acid chloride, DIPEA, THF, rt, overnight, 60%; (d) (i) (1-chloro-2-methyl-1-propen-1-yl)dimethylamine, THF, rt, 1 h; (ii) DIPEA, THF, 40 °C, overnight, 9-33%; (e) methylsulfonyl chloride, DCM, 0 °C to rt, 24 h, 16%.

Syntheses of the acetyl analogues (**11, 13-14, 16, 18**) were secured by the Hantzsch thiazole condensation[40] of bromoketone derivatives **56a-e** with acetylthiourea **57** to afford the desired analogues in good yield. Alternatively, Suzuki-Miyaura cross-coupling of 4-bromo-2-acylaminothiazole **59** with boronic acid **58** using standard palladium cross-coupling conditions afforded the desired product **15** in modest yield (Scheme 2). Analogues (**12**, **17**, **19**) were obtained from commercial suppliers.

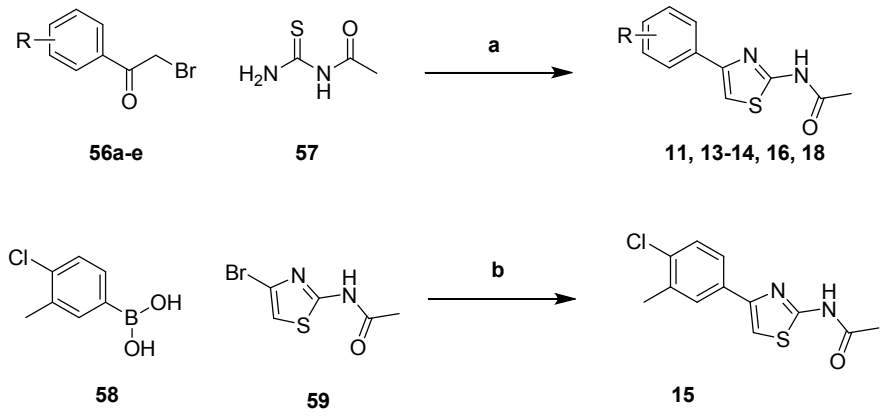

Scheme 2. Modification of Aryl Thiazole

Reagents and conditions: (a) EtOH, microwave, 100-120 °C, 15-20 min or rt, 2.5 h, 6-74%; (b) Pd(dppf)Cl_2, K_2CO_3, iPrOH, microwave, 100 °C, 1 h, 25%.

Heterocycles analogues (**20-27**) were synthesised using standard heterocyclic synthesis methods (see Supporting information for detailed scheme).

The pyrazoline cores **28**, **62** and **65** were assembled by cyclisation of (3,4-dichlorophenyl)hydrazine **60** with the corresponding substituted acrylonitriles under basic conditions. Coupling with a range of acid chloride or carboxylic acid derivatives

delivered the substituted pyrazolines **29-49**, **52** in acceptable yields for biological evaluation (Scheme 3-5).

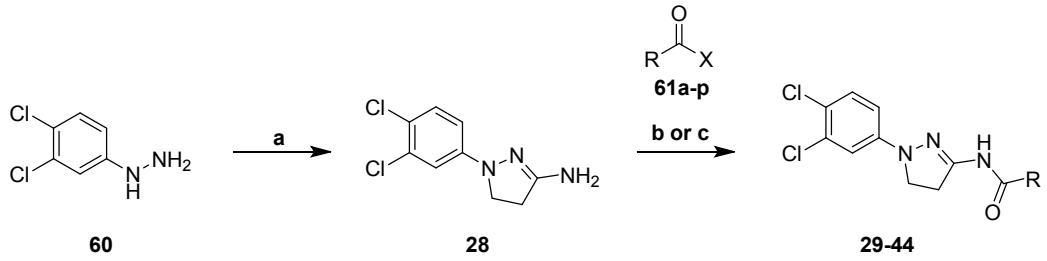

Scheme 3. Modification of the Amide Substituents on the Pyrazoline Core

Reagents and conditions: (a) acrylonitrile, EtOH, NaOEt, 80 °C, nitrogen atm., 19 h, 66%; (b) acid chloride, pyridine, DCM, rt, overnight to 2 days, 2-4%; (c) carboxylic acid, HATU, DIPEA, DCM or DMF, rt, 1 h to 2 days, 1-80%.

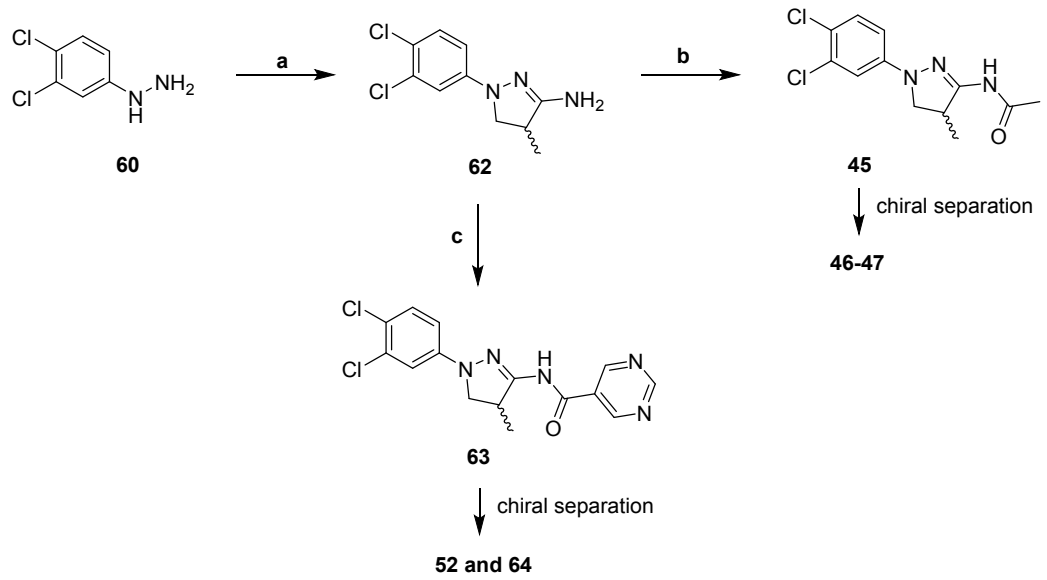

Scheme 4. Substitution of the Pyrazoline Core

Reagents and conditions: (a) 1. NaOEt, EtOH, 80 °C, 5 min, 2. 2-methyl-2-propenenitrile, 85 °C, 2 h, 82%; (b) acetal chloride, pyridine, DCM, rt, 16 h, 30%; (c) 5-pyrimidinecarboxylic acid, HATU, DIPEA, DCM, rt, 2 h, 7%.

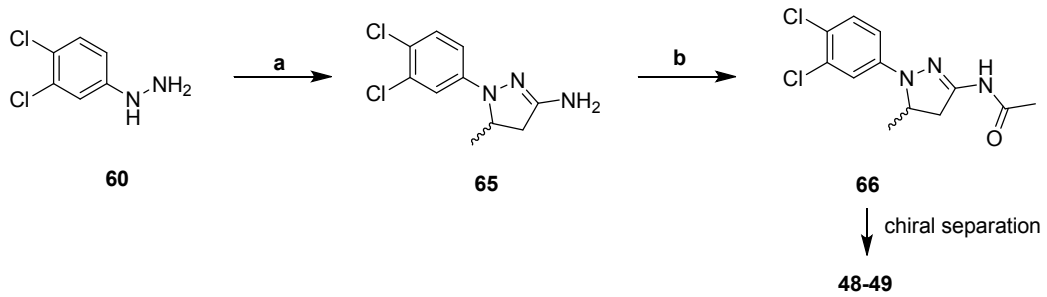

Scheme 5. Substitution of the Pyrazoline Core

Reagents and conditions: (a) crotonitrile, EtOH, NaOEt in EtOH (21 w/w%), reflux, overnight, 36%; (b) acetal chloride, pyridine, DCM, rt, 2 days, sealed vial, 36%.

Compounds **50-51** were synthesised following Scheme 6. Condensation of compound **67** with ethyl cyanoacetate gave intermediate **68** in moderate yield. Reduction of the ester group using lithium borohydride gave the alcohol intermediate **69** in good yield. Mesylation of the alcohol using methanesulfonyl chloride and triethylamine followed by elimination using DBU gave the acrylonitrile intermediate **70** in excellent yield. The aminopyrazoline core **71** was assembled by cyclisation of (3,4-dichlorophenyl)hydrazine **60** with acrylonitrile **70** under basic conditions. Amide coupling using HATU with the appropriate carboxylic acid followed by acid-catalysed deprotection of the THP group gave the final compounds **50** and **51** and good yields.

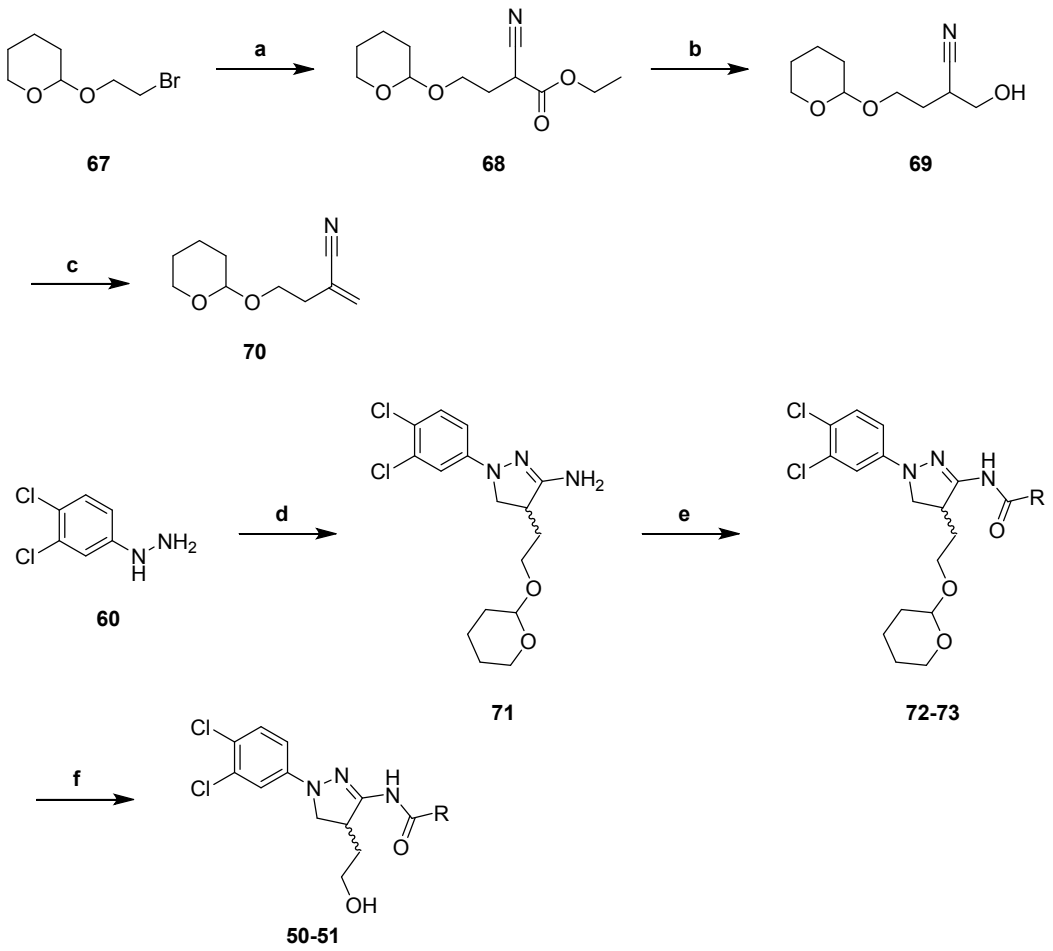

Scheme 6. Substitution of the Pyrazoline Core

*Reagents and conditions: (a) ethyl cyanoacetate, DMF, 70 °C, 2 h followed by rt, 3 days, 50%; (b)$LiBH_4$, THF, 0 °C then rt, overnight, 75%; (c) 1. methanesulfonyl chloride, Et_3N, THF, rt, 1 h, 2. DBU, 60 °C, 1 h followed by rt, 3 h, 96%; (d) 1.NaOEt in EtOH (21 w/w%), EtOH, 80 °C, 5 min, 2. Intermediate **70** in EtOH dropwise, reflux, 3 h followed by rt, overnight, 51%; (e) carboxylic acid, HATU, DIPEA, DCM, 40 °C, overnight; (f) acetic acid, THF/water, 40 °C, 2 days, 51-61% over two steps.*

EXPERIMENTAL SECTION

Chemistry. General. All solvents and reagents, unless otherwise stated, were commercially available from regular suppliers such as Sigma-Aldrich and Fluorochem and were used without further purification. Proton nuclear magnetic resonance (^{1}H NMR) spectra were recorded using a Bruker DPX250, DPX400, AV400 or AVIII600 (with cryoprobe) in the indicated solvent. Chemical shifts δ are reported in parts per million (ppm) relative to tetramethylsilane and are internally referenced to the residual solvent peak. Coupling constants (*J*) are given in hertz (Hz) to the nearest 0.1 Hz. The following abbreviations are used for multiplicities: s=singlet; br.s=broad singlet; d=doublet; t=triplet; m=multiplet; dd=doublet of doublets; ddd=double double doublet. Liquid Chromatography-Mass Spectroscopy (LCMS) was conducted on either a Acquity UPLC BEH C18 column (50 mm x 2.1 mm i.d. 1.7µm packing diameter) at 40 ^{o}C or a HPLC XBridge or Sunfire C18 column (50 mm x 4.6 mm i.d. 3.5 µm packing diameter) at 30 ^{o}C eluting with either 10 mM ammonium bicarbonate in water adjusted to pH 10 with ammonia solution (solvent A) and acetonitrile (solvent B) or 0.1% v/v solution of formic acid in water (solvent A) and 0.1% v/v solution of formic acid in acetonitrile (solvent B). The UV detection is a summed signal from wavelength of 210 nm to 350 nm. The mass spectra were recorded on a Waters ZQ spectrometer using electrospray positive and negative mode. LCMS methods are detailed in the Supporting Information. High resolution mass spectra (HRMS) were obtained on a Micromass Q-Tof 2 hybrid quadrupole time-of-flight mass spectrometer, equipped with a Z-spray interface ESI (+), over a mass range of 100 – 1100 Da, with a scan time of 0.9 s and an interscan delay of 0.1 s. Reserpine was used as the external mass calibrant ($[M+H]^+$ = 609.2812 Da). The Q-Tof 2 mass spectrometer was operated in W reflectron mode to

give a resolution (FWHM) of 16000-20000. Ionisation was achieved with a spray voltage of 3.2 kV, a cone voltage of 50V, with cone and desolvation gas flows of 10-20 and 600 L/h respectively. The source block and desolvation temperatures were maintained at 120 ºC and 250 ºC respectively. The elemental composition was calculated using MassLynx v4.1 for the $[M+H]^+$ and the mass error quoted as ppm. An Agilent 1100 Liquid Chromatograph equipped with a model G1367A autosampler, a model G1312A binary pump and a HP1100 model G1315B diode array detector was used. The method used was generic for all experiments. All separations were achieved using a Phenomenex Luna C18(2) reversed phase column (100 x 2.1 mm, 3µm particle size). Gradient elution was carried out with the mobile phases as (A) water containing 0.1% v/v formic acid and (B) acetonitrile containing 0.1% v/v formic acid. The conditions for the gradient elution were initially 5% B, increasing linearly to 100% B over 6 minutes, remaining at 100% B for 2.5 minutes then decreasing linearly to 5% B over 1 minute followed by an equilibration period of 2.5 minutes prior to the next injection. The flow rate was 0.5 mL/min, temperature controlled at 35ºC with an injection volume of between 2 to 5 µL. All samples were diluted with DMSO (99.9%) prior to LCMS analysis. Analytical chiral chromatography was conducted on a Chiralpak IA, col.no.IAOOCE-MC024 (25 cm) at room temperature eluting with 5% ethanol/heptane (1 mL/min). The UV detection was at 215 nm. Preparative chiral chromatography was conducted on a Chiralpak IA.col.no.IAOOCE-KF008 (25 cm x 2 cm) at room temperature eluting with 5% ethanol/heptane (15mL/min). The UV detection was at 215 nm. Preparative HPLC using a mass directed auto purification (MDAP) was conducted on a Waters *MassLynx* system comprising of a Waters 515 pump with extended pump heads, Waters 2767 autosampler, Waters 996 photodiode array detector and Gilson 202 fraction collector on a XBridge or Sunfire C18 column

(30 mm x 150 mm i.d. 5 μm packing diameter) at ambient temperature. The mobile phase was 0.1% formic acid in water or 10 mM ammonium bicarbonate in water adjusted to pH 10 with ammonia solution (solvent A) and 0.1% formic in acetonitrile or acetonitrile (solvent B). The UV detection is a summed signal from wavelength of 210 nm to 350 nm. Mass spectra were recorded on Waters ZQ mass spectrometer using alternate-scan positive and negative electrospray ionization. The software used was *MassLynx* 3.5 with *FractionLynx* optio or using equivalent alternative systems. MDAP methods are detailed in the Supporting Information. Column chromatography was conducted on a Combiflash® Rf, automated flash chromatography system, from Teledyne Isco using disposable, normal or reverse phase, SPE Redisep cartridges (4 g to 330 g). The CombiFlash® Rf uses RFID (Radio Frequency Identification) technology to automate setting the parameters for purification runs and fraction collection. The system is equipped with a UV variable dual-wavelength and a Foxy® fraction collector enabling automated peak cutting, collection and tracking. Microwave chemistry was typically performed in sealed vessels, irradiating with a suitable microwave reactor system, such as a Biotage Initiator™ Microwave Synthesiser. Solid Phase Extraction (SPE) cartridges from were used to isolate acidic or basic compounds. NH2-SPE refers to aminopropyl solid phase extraction cartridge and SCX-SPE refers to benzenesulphonic acid solid phase extraction cartridge. Isolute® phase separator cartridges sold by Whatman are fitted with hydrophobic Treflon frit and were used to separate chlorinated solvent from aqueous phase under gravity. The purity of all compounds screened in biological assays was examined by LCMS analysis and was found to be ≥ 95% unless otherwise specified. All animal studies were ethically reviewed and carried out in accordance with Animals (Scientific Procedures) Act 1986 and the GSK Policy on the Care, Welfare, and Treatment of Laboratory Animals.

***N*-[4-(3,4-dichlorophenyl)-1,3-thiazol-2-yl]acetamide, 2.** *N*-[4-(3,4-dichlorophenyl)-1,3-thiazol-2-yl]acetamide was prepared following general procedure A using acetic acid (6.6 µL, 0.126 mmol), HATU (48 mg, 0.126 mmol) and DIPEA (0.044 mL, 0.252 mmol) in DMF (1 mL). The reaction was stirred at 50 ºC for 30 min before addition of 4-(3,4-dichlorophenyl)-1,3-thiazol-2-amine (34 mg, 0.139 mmol). The reaction mixture was heated at 50 ºC for 65 h. The reaction mixture was passed through an ion exchange SCX-SPE column (1 g) and the product was eluted with MeOH. The residue was purified by preparative HPLC (method C, formic, 10 min) to provide the title compound (4.7 mg, 13% yield). LCMS (2 min, formic): R_t=1.15 min, $[M+H]^+$=287.0; ^{1}H NMR (600 MHz, DMSO-d_6) δ 12.27 (br. s, 1H), 8.12 (d, *J* = 1.3 Hz, 1H), 7.87 (dd, *J* = 1.3, 8.4 Hz, 1H), 7.81 (s, 1H), 7.69 (d, *J* = 8.4 Hz, 1H), 2.16 (s, 3H).

2-Cyano-*N*-[4-(3,4-dichlorophenyl)-1,3-thiazol-2-yl]acetamide, 6. Activated cyanoacetic acid was made by adding cyanoacetic acid (107 mg, 1.264 mmol) and (1-chloro-2-methyl-1-propen-1-yl)dimethylamine (184 mg, 1.378 mmol) into a vial with THF (4 mL). The mixture was left stirring for 1 h and 4-(3,4-dichlorophenyl)-1,3-thiazol-2-amine (282 mg, 1.149 mmol) and DIPEA (0.602 ml, 3.45 mmol) were added. The reaction was left stirring for 16 h at 50 °C. The reaction was then heated at 70 °C for 3 h. Another 0.5 equivalents of activated acid was added (this was done by making a second stock solution with 107 mg cyanoacetic acid and 184mg (1-chloro-2-methyl-1-propen-1-yl)dimethylamine in 2 mL THF and leaving it to stir for 1 h). The reactions was left at 70 °C for 16 h. THF was removed. Water, saturated aqueous sodium bicarbonate and DCM were added. The organic layer was separated and the aqueous layer was further extracted with DCM. The combined organic layers were concentrated.

The resulting solid was recrystallised using ether, ethyl acetate and 2 drops of DCM to give the title compound as yellow crystals (34 mg, 9% yield). LCMS (method A): R_t = 1.15 min, $[M+H]^+$ = 312.04; ^{1}H NMR (400 MHz, METHANOL-d_4) δ 8.07 (d, *J* = 2.0 Hz, 1H), 7.81 (dd, *J* = 2.0, 8.5 Hz, 1H), 7.50-7.57 (m, 2H), 3.91 (s, 2H); HRMS (ESI) calcd for $C_{12}H_7Cl_2N_3OS+H^+$ 311.9765, found 311.9765 (5.70 min).

1-(3,4-Dichlorophenyl)-4,5-dihydro-1H-pyrazol-3-amine, 28. 3,4-Dichlorophenylhydrazine hydrochloride (10 g, 46.8 mmol) was dissolved in degassed EtOH (50 mL) and treated with acrylonitrile (4.63 mL, 70.3 mmol) and sodium ethoxide in EtOH (21 w/w%, 35 mL, 94 mmol). The reaction was heated at 80 ºC under an atmosphere of nitrogen for 19 h. The reaction was cooled to room temperature and the solid which had formed was collected by filtration, washed with EtOH and water and dried in a vacuum oven to give the title compound as a brown solid (7.14 g, 66%). LCMS (2 min, formic): R_t=0.86 min, $[M+H]^+$=229.8; ^{1}H NMR (400 MHz, DMSO-d_6) δ 7.27 (d, *J* = 8.8 Hz, 1H), 6.89 (d, *J* = 2.8 Hz, 1H), 6.66 (dd, *J* = 2.6, 8.9 Hz, 1H), 5.91 (s, 2H), 3.53 (t, *J* = 9.3 Hz, 2H), 2.81 (t, *J* = 9.3 Hz, 2H).

***N*-[1-(3,4-dichlorophenyl)-4,5-dihydro-1*H*-pyrazol-3-yl]acetamide, 29.** 1-(3,4-Dichlorophenyl)-4,5-dihydro-1*H*-pyrazol-3-amine **28** (500 mg, 2.17 mmol) was dissolved in DCM (20 mL) and treated with acetyl chloride (309 µL, 4.35 mmol) and pyridine (527 µL, 6.52 mmol). The reaction was stirred at room temperature overnight. 2 M aqueous HCl solution (100 mL) was added and product was extracted with DCM (3 x 50 mL). The combined organics were concentrated. The crude product was purified by normal phase chromatography (SiO_2, 30-70% EtOAc/cyclohexane) to give crude desired product. The crude material was then triturated with water to give the title

compound (26 mg, 4% yield). LCMS (2 min, formic): R_t=1.02 min, $[M+H]^+$=272.1; ^{1}H NMR (400 MHz, DMSO-d_6) δ 10.72 (br. s, 1H), 7.39 (d, *J* = 8.8 Hz, 1H), 7.02 (d, *J* = 2.5 Hz, 1H), 6.80 (dd, *J* = 2.5, 8.8 Hz, 1H), 3.65 - 3.75 (m, 2H), 3.34 - 3.40 (m, 2H), 2.01 (s, 3H).

2-Cyano-*N*-[1-(3,4-dichlorophenyl)-4,5-dihydro-1*H*-pyrazol-3-yl]acetamide, 30. Cyanoacetic acid (0.739 g, 8.69 mmol) was dissolved in DCM (70 mL) and treated with HATU (4.96 g, 13.04 mmol) and DIPEA (4.55 mL, 26.1 mmol), followed by 1-(3,4-dichlorophenyl)-4,5-dihydro-1*H*-pyrazol-3-amine **28** (2 g, 8.69 mmol). The reaction mixture was stirred at room temperature overnight. Due to incomplete reaction, cyanoacetic acid (0.739 g, 8.69 mmol) and HATU (4.96 g, 13.04 mmol) were added to the mixture and stirred overnight. The insoluble materials were removed by filtration. The filtrate was partitioned between 2 M aqueous sodium bicarbonate solution (30 mL) and DCM (30 mL). The layers were separated and the aqueous was washed with further DCM (10 mL). The combined organics were evaporated. 200 mg of crude were purified by HPLC (method C, high pH, 10 min) to give the desired product (13.2 mg, 0.5% yield). LCMS (2 min, formic): R_t=1.05 min, $[M+H]^+$ =296.9; ^{1}H NMR (400 MHz, METHANOL-d_4) δ 7.97 (s, 1H), 7.26 (d, *J* = 8.8 Hz, 1H), 7.06 (d, *J* = 2.5 Hz, 1H), 6.79 (dd, *J* = 2.5, 8.8 Hz, 1H), 3.67 - 3.79 (m, 2H), 3.37 - 3.50 (m, 2H), 2.98 (s, 1H), 2.85 (s, 1H); HRMS (ESI) calcd for $C_{12}H_{10}N_4OCl_2$ + H^+ 297.0310, found 297.0304 (5.47min).

3-cyano-*N*-(1-(3,4-dichlorophenyl)-4,5-dihydro-1*H*-pyrazol-3-yl)propanamide, 32. 3-Cyanopropanoic acid (26.0 mg, 0.261 mmol), HATU (165 mg, 0.435 mmol) and DIPEA (0.114 mL, 0.652 mmol) in DCM (2 mL) were stirred at room temperature for

30 min. 1-(3,4-dichlorophenyl)-4,5-dihydro-1*H*-pyrazol-3-amine **28** (50 mg, 0.217 mmol) was then added and the reaction mixture was stirred at room temperature overnight. Saturated aqueous sodium bicarbonate was added to the mixture and the phases were separated using hydrophobic frit. The organic phase was concentrated under a stream of nitrogen. The resulting crude product was purified by preparative HPLC (method C, formic, 10 min) to give the title compound (21.9 mg, 31% yield). LCMS (2 min, formic): R_t=1.08 min, $[M+H]^+$=311.0; ^{1}H NMR (400 MHz, DMSO-d_6) δ 10.89 (br. s, 1H), 7.40 (d, *J* = 9.0 Hz, 1H), 7.03 (d, *J* = 2.5 Hz, 1H), 6.81 (dd, *J* = 2.5, 8.9 Hz, 1H), 3.72 (t, *J* = 9.8 Hz, 2H), 3.37 (t, *J* = 9.8 Hz, 2H), 2.68 (br. s, 4H).

***N*-[1-(3,4-dichlorophenyl)-4-methyl-4,5-dihydro-1*H*-pyrazol-3-yl]acetamide, 45 (racemic), 46 (enantiomer 1) and 47 (enantiomer 2).** *N*-[1-(3,4-dichlorophenyl)-4-methyl-4,5-dihydro-1*H*-pyrazol-3-yl]acetamide was prepared following general procedure C using acetyl chloride (0.040 mL, 0.565 mmol), amine 1-(3,4-dichlorophenyl)-4-methyl-4,5-dihydro-1*H*-pyrazol-3-amine **62** (115 mg, 0.471 mmol) and pyridine (0.076 mL, 0.942 mmol) in DCM (0.8 mL). The reaction was stirred for 32 h at room temperature. The reaction mixture was concentrated and purified by preparative HPLC (method C, high pH, 10 min) to give the title compound as a white solid (29 mg, 30% yield, racemic **45**). LCMS (5 min, high pH): R_t=2.91 min, $[M+H]^+$=285.9; ^{1}H NMR (400 MHz, CHLOROFORM-d) δ 7.77 (br. s, 1H), 7.26 (d, *J* = 8.8 Hz, 1H), 7.00 (d, *J* = 2.8 Hz, 1H), 6.71 (dd, *J* = 2.8, 8.8 Hz, 1H), 4.04 (br. s, 1H), 3.67 - 3.78 (m, 1H), 3.59 (br. s, 1H), 2.16 (br. s, 3H), 1.31 (d, *J* = 7.0 Hz, 3H). The two enantiomers were separated using reverse phase chiral chromatography (heptane:EtOH 8:2) to afford the two desired enantiomers. Enantiomer 1 as a white solid (**46** - 10.8 mg, 8% yield, absolute stereochemistry not assigned - (*R*)-enantiomer assigned from X-ray

crystallography by analogy): chiral HPLC (5% EtOH/heptane): R_t=5.709 min; LCMS (2 min, formic): R_t=1.07 min, $[M+H]^+$=285.8; ^{1}H NMR (400 MHz, DMSO-d_6) δ 10.53 (br. s, 1H), 7.40 (d, *J* = 8.8 Hz, 1H), 7.05 (d, *J* = 2.8 Hz, 1H), 6.82 (dd, *J* = 2.8, 8.8 Hz, 1H), 3.82 (br. s, 1H), 3.55 - 3.74 (m, 2H), 2.03 (s, 3H), 1.17 (d, *J* = 7.0 Hz, 3H). Enantiomer 2 as a white solid (**47 -** 11.8 mg, 8.7% yield, absolute stereochemistry not assigned (*S*)-enantiomer assigned from X-ray crystallography): chiral HPLC (5% EtOH/heptane): R_t=7.155 min; LCMS (2 min, formic): R_t= 1.07 min, $[M+H]^+$=285.8; ^{1}H NMR (400 MHz, DMSO-d_6) δ 10.53 (br. s, 1H), 7.40 (d, *J* = 8.8 Hz, 1H), 7.04 (d, *J* = 2.7 Hz, 1H), 6.82 (dd, *J* = 2.7, 8.8 Hz, 1H), 3.82 (br. s, 1H), 3.56 - 3.74 (m, 2H), 2.03 (s, 3H), 1.17 (d, *J* = 7.0 Hz, 3H).

rac-*N*-[1-(3,4-dichlorophenyl)-4-(2-hydroxyethyl)-4,5-dihydro-1*H*-pyrazol-3-yl]-4-pyridinecarboxamide, 51. A solution of *N*-{1-(3,4-dichlorophenyl)-4-[2-(tetrahydro-2*H*-pyran-2-yloxy)ethyl]-4,5-dihydro-1*H*-pyrazol-3-yl}-4-pyridinecarboxamide **71** (388 mg, 0.84 mmol) in THF (3 mL), water (1.5 mL) and acetic acid (3 mL) was stirred at 40 ºC for 2 days. The mixture was basified with saturated aqueous sodium bicarbonate solution (50 mL), then extracted with DCM (3 x 100 mL). The combined organic solution was evaporated and dried over Na_2SO_4, filtered and concentrated under reduced pressure. The residue was purified by normal phase chromatography (SiO_2, 50-100% EtOAc/DCM) to give the title compound (194.1 mg, 61% yield). LCMS (2 min, formic): R_t=0.94 min, $[M+H]^+$=378.9; ^{1}H NMR (400 MHz, DMSO-d_6) δ 11.27 (br. s, 1H), 8.74 - 8.81 (m, 2H), 7.83 - 7.89 (m, 2H), 7.44 (d, *J* = 9.0 Hz, 1H), 7.14 (d, *J* = 2.5 Hz, 1H), 6.92 (dd, *J* = 2.5, 9.0 Hz, 1H), 4.66 (br. s, 1H), 3.95 - 4.05 (m, 1H), 3.87 (dd, *J* = 5.0, 10.3 Hz, 1H), 3.76 (t, *J* = 10.3 Hz,

1H), 3.52 (t, *J* = 6.6 Hz, 2H), 1.78 - 1.89 (m, 1H), 1.51 - 1.63 (m, 1H); HRMS (ESI) calcd for $C_{17}H_{16}Cl_2N_4O_2$+H^+ 379.0729, found 379.0719 (4.85 min).

***N*-[1-(3,4-dichlorophenyl)-4-methyl-4,5-dihydro-1*H*-pyrazol-3-yl]-5-pyrimidinecarboxamide, 52.** A mixture of 5-pyrimidinecarboxylic acid (0.763 g, 6.14 mmol), HATU (3.12 g, 8.19 mmol) and DIPEA (2.146 mL, 12.29 mmol) in DCM (50 mL) was stirred at room temperature for 30 min. 1-(3,4-Dichlorophenyl)-4-methyl-4,5-dihydro-1H-pyrazol-3-amine **62** (1 g, 4.10 mmol) was then added and the reaction mixture was stirred at room temperature for 2 h. The reaction was quenched with aqueous $NaHCO_3$ solution then extracted with DCM. The organic layer was evaporated. The residue was purified by normal phase chromatography (SiO_2, DCM/EtOAc 3:1 to 1:1) to give the title compound as a racemic mixture (**63** - 96.8 mg, 7% yield). LCMS (2 min, high pH): R_t= 1.09 min, $[M+H]^+$=349.9. The two enantiomers were separated using reverse phase chiral chromatography (EtOH) to afford the two desired enantiomers. Enantiomer 1 (prefered enantiomer **52**): chiral HPLC (EtOH): R_t=16 min; LCMS (2 min, formic): R_t=1.09 min, $[M+H]^+$=349.9; 1H NMR (400 MHz, DMSO-d_6) δ 11.42 (s, 1H), 9.36 (s, 1H), 9.26 (s, 2H), 7.44 (d, *J* = 9.1 Hz, 1H), 7.13 (d, *J* = 2.5 Hz, 1H), 6.90 (dd, *J* = 2.8, 8.8 Hz, 1H), 3.92 - 4.08 (m, 1H), 3.81 (t, *J* = 10.1 Hz, 1H), 3.70 (dd, *J* = 4.8, 9.8 Hz, 1H), 1.24 (d, *J* = 7.1 Hz, 3H). Enantiomer 2 (non-prefered enantiomer **64**): chiral HPLC (EtOH): R_t=44 min; LCMS (2 min, formic): R_t=1.09 min, $[M+H]^+$=349.9; 1H NMR (400 MHz, DMSO-d6) δ 11.42 (s, 1H), 9.36 (s, 1H), 9.26 (s, 2H), 7.44 (d, *J* = 9.1 Hz, 1H), 7.13 (d, *J* = 2.5 Hz, 1H), 6.90 (dd, *J* = 2.8, 8.8 Hz, 1H), 3.92 - 4.08 (m, 1H), 3.81 (t, *J* = 10.1 Hz, 1H), 3.70 (dd, *J* = 4.8, 9.8 Hz, 1H), 1.24 (d, *J* = 7.1 Hz, 3H).

4-(3,4-Dichlorophenyl)thiazol-2-amine, 54. 2-Bromo-1-(3,4-dichlorophenyl)ethanone (5 g, 18.66 mmol) and thiourea (1.421 g, 18.66 mmol) were stirred in EtOH (60 mL). After 10 min, white solid had formed and the reaction was seen as complete. The resulting solid was filtered and washed with EtOAc. The product was dried in a vacuum oven over the weekend. The crude product was ground into a fine powder then washed twice with water to give the title product (3.87 g, 85% yield). LCMS (2 min, formic): R_t=1.03 min, $[M+H]^+$=245.0. ^{1}H NMR (400 MHz, DMSO-d_6) δ 8.02 (d, *J* = 2.0 Hz, 1H), 7.76 (dd, *J* = 2.0, 8.5 Hz, 1H), 7.66 (d, *J* = 8.5 Hz, 1H), 7.29 (s, 1H).

1-(3,4-Dichlorophenyl)-4-methyl-4,5-dihydro-1*H*-pyrazol-3-amine, 62. To a suspension of 3,4-dichlorophenylhydrazine hydrochloride (32 g, 150 mmol) in EtOH (75 mL) at room temperature, sodium ethoxide in EtOH (21 w/w%, 67.1 mL, 180 mmol) was added dropwise. The mixture was stirred at 80 ºC for 5 min and cooled to room temperature. To the mixture, 2-methyl-2-propenenitrile (13.83 mL, 165 mmol) was added dropwise and refluxed at 85 ºC for 2 h. The mixture was cooled to room temperature then water (500 mL) was added. The resulting suspension was evaporated to remove EtOH then the formed solid was collected by filtration. The solid was washed with water (x 5) then dried under reduced pressure to give the title product (30.1 g, 82% yield). LCMS (2 min, formic): R_t=0.95 min, $[M+H]^+$=243.8 (93% purity); ^{1}H NMR (400 MHz, CHLOROFORM-d) δ 7.18 - 7.38 (m, 1H), 7.01 (d, *J* = 2.5 Hz, 1H), 6.73 (dd, *J* = 2.5, 8.8 Hz, 1H), 4.08 (br. s, 2H), 3.83 - 3.96 (m, 1H), 3.08-3.35 (m, 2H), 1.35 (d, *J* = 6.8 Hz, 3H).

1-(3,4-Dichlorophenyl)-4-[2-(tetrahydro-2*H*-pyran-2-yloxy)ethyl]-4,5-dihydro-1*H*-pyrazol-3-amine, 71. To a suspension of 3,4-dichlorophenylhydrazine hydrochloride **60** (2.35 g, 11.0 mmol) in EtOH (11 mL) at room temperature, sodium ethoxide in EtOH (21 w/w%, 4.94 mL, 13.22 mmol) was added dropwise. The mixture was stirred at 80 ºC for 5 min and cooled to room temperature. To the mixture, 2-[2-(tetrahydro-2*H*-pyran-2-yloxy)ethyl]-2-propenenitrile **70** (2.0 g, 11.0 mmol) in EtOH (11 mL) was added dropwise. The mixture was refluxed for 3 h then stirred at room temperature overnight. Water (100 mL) was added, then extracted with DCM (3 x 200 mL). The combined organics were dried over Na_2SO_4, filtered and concentrated under reduced pressure. The residue was purified by normal phase chromatography (SiO_2, DCM/EtOAc 20:1 ~ 1:2) to give the title compound as a diastereomer mixture (2.27 g, 57% yield). LCMS (2 min, formic): R_t=1.16 min, $[M+H]^+$=357.9; ^{1}H NMR (400 MHz, DMSO-d_6) δ 7.25 - 7.30 (m, 1H), 6.90 (d, *J* = 2.5 Hz, 1H), 6.67 (dd, *J* = 2.5, 8.9 Hz, 1H), 5.86 (br, 2H), 4.53 - 4.61 (m, 1H), 3.63 - 3.79 (m, 3H), 3.38 - 3.48 (m, 2H), 3.32 - 3.38 (m, 1H), 3.08 - 3.22 (m, 1H), 2.02 - 2.15 (m, 1H), 1.55 - 1.79 (m, 3H), 1.33 - 1.55 (m, 4H).

***N*-{1-(3,4-dichlorophenyl)-4-[2-(tetrahydro-2*H*-pyran-2-yloxy)ethyl]-4,5-dihydro-1*H*-pyrazol-3-yl]-4-pyridinecarboxamide, 73.** *N*-{1-(3,4-dichlorophenyl)-4-[2-(tetrahydro-2*H*-pyran-2-yloxy)ethyl]-4,5-dihydro-1*H*-pyrazol-3-yl}-4-pyridinecarboxamide was prepared following general procedure A using 4-pyridinecarboxylic acid (155 mg, 1.26 mmol), HATU (541 mg, 1.42 mmol) and DIPEA (0.44 mL, 2.51 mmol) in DCM (9 mL). The mixture was stirred at room temperature for 5 min before addition of 1-(3,4-dichlorophenyl)-4-[2-(tetrahydro-2*H*-pyran-2-yloxy)ethyl]-4,5-dihydro-1*H*-pyrazol-3-amine **71** (300 mg, 0.84 mmol). The mixture

was stirred at 40 ºC overnight. The reaction was quenched with saturated aqueous sodium bicarbonate solution (50 mL), then extracted with DCM (3 x 100 mL). The combined organics were dried over Na_2SO_4, filtered and concentrated in vacuo. The residue was purified by normal phase chromatography (SiO_2, 30-95% EtOAc/DCM) to give the title compound (388 mg, quantitative yield). LCMS (2 min, formic) R_t=1.23 min, $[M+H]^+$=462.9; ^{1}H NMR (400 MHz, DMSO-d_6) δ 11.30 (br. s, 1H), 8.74 - 8.82 (m, *J* = 6.0 Hz, 2H), 7.85 - 7.88 (m, 2H), 7.44 (d, *J* = 9.1 Hz, 1H), 7.14 (d, *J* = 2.5 Hz, 1H), 6.88 - 6.94 (m, 1H), 4.51 - 4.57 (m, 1H), 3.98 - 4.15 (m, 1H), 3.86 - 3.98 (m, 1H), 3.59 - 3.85 (m, 3H), 3.41 - 3.50 (m, 1H), 1.87 - 2.01 (m, 1H), 1.19 - 1.82 (m, 7H), 1H assumed to be overlapped with a water peak.

Physicochemical Studies.

Chemiluminescent Nitrogen Detection (CLND) Solubility Determination. GSK in-house kinetic solubility assay involved the following: 5 µL of 10 mM DMSO stock solution diluted to 100 µL with pH 7.4 phosphate buffered saline, equilibrated for 1 h at room temperature, filtered through Millipore MultiscreenHTS-PCF filter plates (MSSL BPC). The filtrate is quantified by suitably calibrated flow injection chemi-luminescent nitrogen detection.[42] The standard error of the CLND solubility determination is ±30 µM, the upper limit of the solubility is 500 µM when working from 10 mM DMSO stock solution.

Artificial Membrane Permeability assay. The donor cell contained 2.5 µL of 10 mM sample solution in pH 7.05 phosphate buffer. To enhance solubility, 0.5% hydroxypropyl-cyclodextrin (encapsin) has been added to the buffer. The artificial membrane is prepared from 1.8% phosphatidylcholine and 1% cholesterol in decane solution. The sample concentration in both the donor and acceptor compartment is

determined by LC-MS after 3 h incubation at room temperature.[43] The permeability (logPapp) measuring how fast molecules pass through the black lipid membrane is expressed in nm/s. The average standard error of the assay is around ±30 nm/s that can be higher at the low permeability range.

Biology.

IMAP enzyme activation assay. Procedure reported by J. Cottom *et al.*[24]

Fluorescence Polarisation Binding assay (FP). Procedure reported by J. Yang *et al.*[17]

Cell Lysis and Western Blot.[17] Cells were lysed in 10 mM sodium phosphate buffer, pH 7.1, containing 1% Triton X100,0.05% SDS, 150 mM NaCl, 1X complete protease Inhibitor cocktail (Roche, Indianapolis), 2X PhosSTOP phosphatase Inhibitor Cocktail (Roche, Indianapolis) and 1µg/ml Pepstatin A (Roche, Indianapolis). After 10 min incubation on ice, cells were centrifuged at 14,000g for 10 min and the supernatant was collected. Protein concentration was measured using Bio-Rad protein assay reagent. Thirty five µg of total protein isolated from the cells was resolved on 4-12% SDS-PAGE and electroblotted to a nitrocellulose membrane. Membranes were blocked in Odyssey blocking buffer (LI-COR Biosciences) and incubated overnight at 4 °C with antibodies against c-Abl (SantaCruz; SC-23, Dilution 1:600), pY245 c-Abl (BioSource; Cat# 44-250, Dilution 1:1000), pY412 c-Abl (ECM Bioscience, Dilution 1:1000), pY207 Crk-L/pY221 Crk (Cell Signaling, Dilution 1: 1000), Crk/Crk-L (BD BioScience, Dilution 1:5000). Membranes were washed and subsequently incubated in secondary antibodies alexaflour-680 and Anti-mouse alexaflour-800 and scanned and quantitated using Odyssey Infrared Imaging System (LI-COR Biosciences). Ratio of pCrk/total Crk in compound treated to that of DMSO control ratio was used to calculate the fold induction in Crk phosphorylation.

Pharmacokinetic Studies.

Mouse *In vitro* metabolic stability (Intrinsic Clearance). Pooled CD1 mouse liver microsomes (final protein concentration 0.5 mg/mL), 0.05 M phosphate buffer pH 7.4 and test compound (final substrate concentration 0.5 µM; final DMSO concentration 0.25 %) were pre-incubated at 37 °C prior to the addition of NADPH (final concentration 1 mM) to initiate the reaction. The final incubation volume was 500 µL. A minus cofactor control incubation was included for each compound tested where 0.05 M phosphate buffer pH 7.4 was added instead of NADPH (minus NADPH). Each compound was incubated for 0, 5, 15, 30, 45 and 60 min. The control (minus NADPH) was incubated for 60 min only. The reactions were stopped by transferring 50 µL of incubate to 100 µL of acetonitrile containing internal standard at the appropriate time points. The termination plates were centrifuged at 2,500 rpm for 20 min at 4 °C to precipitate the protein and samples analysed by LC-MS/MS. From a plot of ln peak area ratio (compound peak area/internal standard peak area) against time, the gradient of the line was determined. Subsequently, half-life and intrinsic clearance were calculated using the equations below:

Elimination rate constant (k) = (- gradient)

Half-life ($t_{½}$)(min) = $\frac{0.693}{k}$

Intrinsic clearance (CLint)(mL/min/mg protein) = $\frac{V \times 0.693}{t_{½}}$

where V = Incubation volume (mL)/Microsomal protein (mg)

Relevant control compounds were assessed. Calculated intrinsic clearance values were compared with the GSK data library for each control to confirm the appropriate activity of the batch.

***In vivo* PK Studies.** CD-1 mice were housed as groups of four animals in autoclaved Techniplast Type2 cages containing IPS Lignocel BK8/15 bedding with Datesand Paper Shaving nesting material, red Perspex dome home, cardboard fun tunnel, rodent

running wheel and wooden chew blocks provided. Animals were maintained under a specified pathogen free (SPF) environment in a dedicated rodent animal facility at GlaxoSmithKline (GSK), with an ambient temperature of 20.5 °C to 23.5 °C and relative humidity of 39% to 61%, maintained on a 06:00 to 20:00 light–dark cycle, with free access to food (Labdiet Irradiated 5LF2 Maintenance Diet) and animal grade drinking water. All animal studies were ethically reviewed and carried out in accordance with Animals (Scientific Procedures) Act 1986 and the GSK Policy on the Care, Welfare and Treatment of Laboratory Animals.

Crystallisation and Crystallography Material and Methods.

Protein production for crystallography studies. Protein expression and purification was described in detail in the previous publication describing compound **1**.[17] In Brief, C-abl(248-531)TEV-6xHis was expressed in insect cells with 25 µM Imatinib. Cells were lysed and centrifuged. The supernatant was mixed with Ni-NTA resin, washed and eluted with imidazole. The eluted protein was dialysed to remove the imidazole and cleaved with TEV protease at the same time. The protein was passed over the Ni-NTA resin to remove the tag. Further purification was done on a MonoQ and Superdex 200 columns, respectively. The protein was > 95% pure and stored in 20 mM Tris-HCL, pH 8, 100 mM NaCl, 3mM DTT, and 5% glycerol.

Crystallisation. c-Abl kinase domain (248-531) was incubated with 5x molar excess compound of interest over night. The sample was concentrated to 25mgs/mL and setup as a hanging drop vapor diffusion experiment. The reservoir solution contained 1% - 3% PEG 300, 0.1 M HEPES pH 7.5 and 2M AmSO4. Drops were set up with 200 nL of protein, 200 nL of reservoir at 4 °C. Crystals were harvested from the drop and quickly washed with a reservoir solution contain 15% - 30% glycerol and flash-frozen

in liquid nitrogen. Crystals were stored in an ACTOR puck for shipment to a synchrotron for high-resolution x-ray diffraction data collection.

X-ray data collection and crystal structure determination. X-ray data collection experiments are summarized in Table S1. X-ray diffraction data were integrated and scaled with the XDS package[44] and CCP4 package.[45,46] Molecular replacement solutions were found with PHASER[47] and refinement was done with Phenix.[48] Model building was done with COOT[49] and figures were made with PyMol (http://pymol.sourceforge.net).

Computational modelling using multi-component solvent search (MCSS). See previously published work by Hong X. *et al.*[33]

ASSOCIATED CONTENT

Supporting Information

The Supporting Information is available free of charge on the ACS Publications website at http://pubs.acs.org.

- Complete experimental information for all other intermediates and final compounds whose procedures are not included in the main article; LCMS and MDAP methods; melting point method and data for compounds **9** and **35**; X-ray crystallography table of statistics for compounds **6**, **29** and **51**.
- Molecular formula strings and biological data for compounds **1-52**.

Accession Codes

The final crystal structures are deposited in the Protein Data Bank under the accession codes 6NPE (**6**), 6NPU (**29**) and 6NPV (**51**).

AUTHOR INFORMATION

Corresponding Author

*Dr Sophie M. Bertrand: email: sophie.x.bertrand@gsk.com.

ORCID

Sophie M. Bertrand: 0000-0002-7159-1157

Jennifer A. Borthwick: 0000-0002-6740-4232

Robert J. Young: 0000-0002-7763-0575

Present Addresses

⊥Graham L. Simpson – GTN Ltd, 4-5 Bonhill Street, London, EC2A 4BX, UK.

ǁHelen L. Evans – ImmunoGen, Inc., 830 Winter Street, Wlatham, MA 02451-1477, US.

Notes

The authors declare no competing financial interest: All authors were employees of GlaxoSmithKline at the time the work was carried out.

ACKNOWLEDGEMENTS

The authors acknowledge physicochemical characterisation of the compounds in this paper by Klara Valko, Alan Hill, Shenaz Bunally. The authors acknowledge discussions around the content of the manuscript by Ian Churcher.

ABBREVIATIONS USED

AMP, artificial membrane assay; ATP, adenosine triphosphate; c-Abl, abelson kinase; CLND, chemiluminescent nitrogen detection; CML, chronic mylogenous leukaemia; DBU, 1,8-diazabicyclo[5.4.0]undec-7-ene; DCM, dichloromethane; DHP, dihydropyrazole; DIPEA, *N*,*N*-diisopropylethylamine; DMF, *N,N*-dimethylformamide;

DMSO, dimethylsulfoxide; FP, fluorescence polarisation; HATU, 1-[bis(dimethylamino)methylene]-1*H*-1,2,3-triazolo[4,5-b]pyridinium 3-oxid hexafluorophosphate; HOBt, hydroxybenzotriazole; HPLC, high performance liquid chromatography; IMAP, immobilized metal affinity for phosphochemicals; IPA, propan-2-ol; PFI, property forecast index; Ph1, Philadelphia chromosome; SAR, structure-activity relationship; SPE, solid phase extraction cartridges marketed by Isolute®; THF, tetrahydrofuran; UPLC, ultra performance liquid chromatography.

REFERENCES

1. Manning, G.; Whyte, D. B.; Martinez, R.; Hunter, T.; Sudarsanam, S. The protein kinase complement of the human genome. *Science* **2002,** 298, 1912-1934.

2. Wang, Z.; Cole, P. A. Catalytic Mechanisms and Regulation of Protein Kinases. *Methods Enzymol.* **2014,** 548, 1-21.

3. Zhang, J.; Yang, P. L.; Gray, N. S. Targeting cancer with small molecule kinase inhibitors. *Nat. Rev. Cancer* **2009,** 9, 28-39.

4. Wu, P.; Nielsen, T. E.; Clausen, M. H. Small-molecule kinase inhibitors: an analysis of FDA-approved drugs. *Drug Discovery Today* **2016,** 21, 5-10.

5. Simpson, G. L.; Hughes, J. A.; Washio, Y.; Bertrand, S. M. Direct small-molecule kinase activation: novel approaches for a new era of drug discovery. *Curr. Opin. Drug Discovery Dev.* **2009,** 12, 585-596.

6. Wang, J. Y. Abl tyrosine kinase in signal transduction and cell-cycle regulation. *Current Opin. Genet. Dev.* **1993,** 3, 35-43.

7. Hughes, T.; Deininger, M.; Hochhaus, A.; Branford, S.; Radich, J.; Kaeda, J.; Baccarani, M.; Cortes, J.; Cross, N. C.; Druker, B. J. Monitoring CML patients responding to treatment with tyrosine kinase inhibitors: review and recommendations

for harmonizing current methodology for detecting BCR-ABL transcripts and kinase domain mutations and for expressing results. *Blood* **2006,** 108, 28-37.

8. Quintas-Cardama, A.; Cortes, J. Molecular biology of bcr-abl1-positive chronic myeloid leukemia. *Blood* **2009,** 113, 1619-1630.

9. Rosti, G.; Castagnetti, F.; Gugliotta, G.; Baccarani, M. Tyrosine kinase inhibitors in chronic myeloid leukaemia: which, when, for whom? *Nat. Rev. Clin. Oncol.* **2017,** 14, 141-154.

10. Weisberg, E.; Manley, P. W.; Cowan-Jacob, S. W.; Hochhaus, A.; Griffin, J. D. Second generation inhibitors of BCR-ABL for the treatment of imatinib-resistant chronic myeloid leukaemia. *Nat. Rev. Cancer* **2007,** 7, 345-356.

11. Hantschel, O.; Nagar, B.; Guettler, S.; Kretzschmar, J.; Dorey, K.; Kuriyan, J.; Superti-Furga, G. A myristoyl/phosphotyrosine switch regulates c-Abl. *Cell* **2003,** 112, 845-857.

12. Nagar, B.; Hantschel, O.; Seeliger, M.; Davies, J. M.; Weis, W. I.; Superti-Furga, G.; Kuriyan, J. Organization of the SH3-SH2 unit in active and inactive forms of the c-Abl tyrosine kinase. *Mol. Cell* **2006,** 21, 787-798.

13. Fallacara, A. L.; Tintori, C.; Radi, M.; Schenone, S.; Botta, M. Insight into the allosteric inhibition of Abl kinase. *J. Chem. Inf. Mod.* **2014,** 54, 1325-1338.

14. Adrian, F. J.; Ding, Q.; Sim, T.; Velentza, A.; Sloan, C.; Liu, Y.; Zhang, G.; Hur, W.; Ding, S.; Manley, P.; Mestan, J.; Fabbro, D.; Gray, N. S. Allosteric inhibitors of Bcr-abl-dependent cell proliferation. *Nat. Chem. Biol.* **2006,** 2, 95-102.

15. Wylie, A. A.; Schoepfer, J.; Jahnke, W.; Cowan-Jacob, S. W.; Loo, A.; Furet, P.; Marzinzik, A. L.; Pelle, X.; Donovan, J.; Zhu, W.; Buonamici, S.; Hassan, A. Q.; Lombardo, F.; Iyer, V.; Palmer, M.; Berellini, G.; Dodd, S.; Thohan, S.; Bitter, H.; Branford, S.; Ross, D. M.; Hughes, T. P.; Petruzzelli, L.; Vanasse, K. G.; Warmuth, M.;

Hofmann, F.; Keen, N. J.; Sellers, W. R. The allosteric inhibitor ABL001 enables dual targeting of BCR-ABL1. *Nature* **2017,** 543, 733-737.

16. Jahnke, W.; Grotzfeld, R. M.; Pellé, X.; Strauss, A.; Fendrich, G.; Cowan-Jacob, S. W.; Cotesta, S.; Fabbro, D.; Furet, P.; Mestan, J.; Marzinzik, A. L. Binding or bending: distinction of allosteric Abl kinase agonists from antagonists by an NMR-based conformational assay. *J. Am. Chem. Soc.* **2010,** 132, 7043-7048.

17. Yang, J.; Campobasso, N.; Biju, M. P.; Fisher, K.; Pan, X. Q.; Cottom, J.; Galbraith, S.; Ho, T.; Zhang, H.; Hong, X.; Ward, P.; Hofmann, G.; Siegfried, B.; Zappacosta, F.; Washio, Y.; Cao, P.; Qu, J.; Bertrand, S.; Wang, D. Y.; Head, M. S.; Li, H.; Moores, S.; Lai, Z.; Johanson, K.; Burton, G.; Erickson-Miller, C.; Simpson, G.; Tummino, P.; Copeland, R. A.; Oliff, A. Discovery and characterization of a cell-permeable, small-molecule c-Abl kinase activator that binds to the myristoyl binding site. *Chem. Biol.* **2011,** 18, 177-186.

18. Rosti, V.; Bergamaschi, G.; Lucotti, C.; Danova, M.; Carlo-Stella, C.; Locatelli, F.; Tonon, L.; Mazzini, G.; Cazzola, M. Oligodeoxynucleotides antisense to c-abl specifically inhibit entry into S-phase of CD34+ hematopoietic cells and their differentiation to granulocyte-macrophage progenitors. *Blood* **1995,** 86, 3387-3393.

19. Caracciolo, D.; Valtieri, M.; Venturelli, D.; Peschle, C.; Gewirtz, A. M.; Calabretta, B. Lineage-specific requirement of c-abl function in normal hematopoiesis. *Science* **1989,** 245, 1107-1110.

20. Allington, T. M.; Galliher-Beckley, A. J.; Schiemann, W. P. Activated Abl kinase inhibits oncogenic transforming growth factor-beta signaling and tumorigenesis in mammary tumors. *FASEB J.* **2009,** 23, 4231-4243.

21. Varzavand, A.; Hacker, W.; Ma, D.; Gibson-Corley, K.; Hawayek, M.; Tayh, O. J.; Brown, J. A.; Henry, M. D.; Stipp, C. S. α3β1 Integrin suppresses prostate cancer metastasis *via* regulation of the Hippo pathway. *Cancer Research* **2016,** 76, 6577-6587.

22. Cabigas, E. B.; Liu, J.; Boopathy, A. V.; Che, P. L.; Crawford, B. H.; Baroi, G.; Bhutani, S.; Shen, M.; Wagner, M. B.; Davis, M. E. Dysregulation of catalase activity in newborn myocytes during hypoxia is mediated by c-Abl tyrosine kinase. *J. Cardiovasc. Pharmacol. Ther.* **2014,** 20, 93-103.

23. Dasgupta, Y.; Koptyra, M.; Hoser, G.; Kantekure, K.; Roy, D.; Gornicka, B.; Nieborowska-Skorska, M.; Bolton-Gillespie, E.; Cerny-Reiterer, S.; Muschen, M.; Valent, P.; Wasik, M. A.; Richardson, C.; Hantschel, O.; van der Kuip, H.; Stoklosa, T.; Skorski, T. Normal ABL1 is a tumor suppressor and therapeutic target in human and mouse leukemias expressing oncogenic ABL1 kinases. *Blood* **2016,** 127, 2131-2143.

24. Cottom, J.; Hofmann, G.; Siegfried, B.; Yang, J.; Zhang, H.; Yi, T.; Ho, T. F.; Quinn, C.; Wang, D. Y.; Johanson, K. Assay Development and high-throughput screening of small molecular c-Abl kinase activators. *J. Biomol. Screening* **2011,** 16, 53-64.

25. Freire, E. Do enthalpy and entropy distinguish first in class from best in class? *Drug Discovery Today* **2008,** 13, 869-874.

26. Meanwell, N. A. Improving drug candidates by design: a focus on physicochemical properties as a means of improving compound disposition and safety. *Chem. Res. Toxicol.* **2011,** 24, 1420-1456.

27. Ritchie, T. J.; Macdonald, S. J. F.; Young, R. J.; Pickett, S. D. The impact of aromatic ring count on compound developability: further insights by examining carbo-

and hetero-aromatic and-aliphatic ring types. *Drug Discovery Today* **2011,** 16, 164-171.

28. Chu, K. A.; Yalkowsky, S. H. An interesting relationship between drug absorption and melting point. *Int. J. Pharm.* **2009,** 373, 24-40.

29. Hill, A. P.; Young, R. J. Getting physical in drug discovery: a contemporary perspective on solubility and hydrophobicity. *Drug Discovery Today* **2010,** 15, 648-655.

30. Young, R. J.; Green, D. V.; Luscombe, C. N.; Hill, A. P. Getting physical in drug discovery II: the impact of chromatographic hydrophobicity measurements and aromaticity. *Drug Discovery Today* **2011,** 16, 822-830.

31. Randall, R.; Eakins, K.; Higgs, G.; Salmon, J.; Tateson, J. Inhibition of arachidonic acid cyclo-oxygenase and lipoxygenase activities of leukocytes by indomethacin and compound BW755C. *Inflammation Research* **1980,** 10, 553-555.

32. Challand, S. R.; Copp, F. C.; Denyer, C. V.; Eakins, K. E.; Walker, J. M. G.; Whittaker, N.; Caldwell, A. G. Pharmaceutical compositions containing 3-Amino-pyrazoline derivatives. EP0022548A1, 1981.

33. Hong, X.; Cao, P.; Washio, Y.; Simpson, G.; Campobasso, N.; Yang, J.; Borthwick, J.; Burton, G.; Chabanet, J.; Bertrand, S. Structure-guided optimization of small molecule c-Abl activators. *J. Comput. Aided Mol. Des.* **2014,** 28, 75-87.

34. Brasher, B. B.; Roumiantsev, S.; Van Etten, R. A. Mutational analysis of the regulatory function of the c-Abl Src homology 3 domain. *Oncogene* **2001,** 20, 7744-7752.

35. Eggert, E.; Hillig, R. C.; Koehr, S.; Stöckigt, D.; Weiske, J.; Barak, N.; Mowat, J.; Brumby, T.; Christ, C. D.; Ter Laak, A.; Lang, T.; Fernandez-Montalvan, A. E.; Badock, V.; Weinmann, H.; Hartung, I. V.; Barsyte-Lovejoy, D.; Szewczyk, M.;

Kennedy, S.; Li, F.; Vedadi, M.; Brown, P. J.; Santhakumar, V.; Arrowsmith, C. H.; Stellfeld, T.; Stresemann, C. Discovery and characterization of a highly potent and selective aminopyrazoline-based *in vivo* probe (BAY-598) for the protein lysine methyltransferase SMYD2. *J. Med. Chem.* **2016,** 59, 4578-4600.

36. Gul'ko, L.; Gorodetskova, N.; Klebanov, B. Synthesis and pharmacological activity of 1-aryl-3-amino-2-pyrazoline derivatives. *Pharm. Chem. J.* **1994,** 28, 255-260.

37. Kim, K. H.; Martin, Y. C.; Norris, B.; Young, P. R.; Carter, G. W.; Haviv, F.; Walters, R. L. Quantitative structure–activity relationship of inhibitors of immune complex-induced inflammation: 1-Phenyl-3-aminopyrazoline derivatives. *J. Pharm. Sciences* **1990,** 79, 609-613.

38. Fort, F. L.; Pratt, M. C.; Carter, G. W.; Lewkowski, J. P.; Heyman, I. A.; Cusick, P. K.; Kesterson, J. W. Heinz bodies, methemoglobinemia, and hemolytic anemia induced in rats by 3-amino-1-[m-(trifluoromethyl)phenyl]-2-pyrazoline. *Fundam. Appl. Toxicol.* **1984,** 4, 216-220.

39. Zhang, J.; Adrian, F. J.; Jahnke, W.; Cowan-Jacob, S. W.; Li, A. G.; Iacob, R. E.; Sim, T.; Powers, J.; Dierks, C.; Sun, F.; Guo, G. R.; Ding, Q.; Okram, B.; Choi, Y.; Wojciechowski, A.; Deng, X.; Liu, G.; Fendrich, G.; Strauss, A.; Vajpai, N.; Grzesiek, S.; Tuntland, T.; Liu, Y.; Bursulaya, B.; Azam, M.; Manley, P. W.; Engen, J. R.; Daley, G. Q.; Warmuth, M.; Gray, N. S. Targeting Bcr-Abl by combining allosteric with ATP-binding-site inhibitors. *Nature* **2010,** 463, 501-506.

40. Duca, M.; Malnuit, V.; Barbault, F.; Benhida, R. Design of novel RNA ligands that bind stem–bulge HIV-1 TAR RNA. *Chem. Commun.* **2010,** 46, 6162-6164.

41. Devos, A.; Remion, J.; Frisque-Hesbain, A. M.; Colens, A.; Ghosez, L. Synthesis of acyl halides under very mild conditions. *Chem. Commun* **1979**, 1180-1181.

42. Bhattachar, S. N.; Wesley, J. A.; Seadeek, C. Evaluation of the chemiluminescent nitrogen detector for solubility determinations to support drug discovery. *J. Pharm. Biomed. Anal.* **2006,** 41, 152-157.

43. Veber, D. F.; Johnson, S. R.; Cheng, H.-Y.; Smith, B. R.; Ward, K. W.; Kopple, K. D. Molecular properties that influence the oral bioavailability of drug candidates. *J. Med. Chem.* **2002,** 45, 2615-2623.

44. Kabsch, W. Integration, scaling, space-group assignment and post-refinement. *Acta Crystallogr., sect D: Biol. Crystallogr.* **2010,** 66, 133-144.

45. Evans, P. Scaling and assessment of data quality. *Acta Crystallogr., sect D: Biol. Crystallogr.* **2006,** 62, 72-82.

46. Vonrhein, C.; Flensburg, C.; Keller, P.; Sharff, A.; Smart, O.; Paciorek, W.; Womack, T.; Bricogne, G. Data processing and analysis with the autoPROC toolbox. *Acta Crystallogr., sect D: Biol. Crystallogr.* **2011,** 67, 293-302.

47. McCoy, A. J.; Grosse-Kunstleve, R. W.; Adams, P. D.; Winn, M. D.; Storoni, L. C.; Read, R. J. Phaser crystallographic software. *J. Appl. Crystallogr.* **2007,** 40, 658-674.

48. Adams, P. D.; Afonine, P. V.; Bunkoczi, G.; Chen, V. B.; Davis, I. W.; Echols, N.; Headd, J. J.; Hung, L. W.; Kapral, G. J.; Grosse-Kunstleve, R. W.; McCoy, A. J.; Moriarty, N. W.; Oeffner, R.; Read, R. J.; Richardson, D. C.; Richardson, J. S.; Terwilliger, T. C.; Zwart, P. H. PHENIX: a comprehensive Python-based system for macromolecular structure solution. *Acta Crystallogr., sect D: Biol. Crystallogr.* **2010,** 66, 213-221.

49. Emsley, P.; Cowtan, K. Coot: model-building tools for molecular graphics. *Acta Crystallogr., sect D: Biol. Crystallogr.* **2004,** 60, 2126-2132.

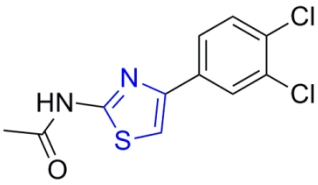

2
FP Binding pIC_{50}: **6.5**
Cell Act pEC_{50}: **4.5**
HTS Hit

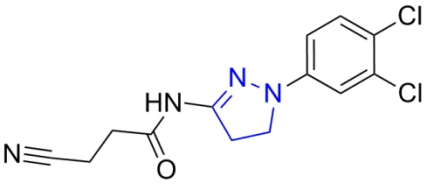

32
FP Binding pIC_{50}: **6.5**
Cell Act pEC_{50}: **6.1**
Showed *in vivo* target engagement and pathway activation

Table of Contents Graphic

130x49mm (300 x 300 DPI)